

The influence of near surface sediment hydrothermalism on the TEX₈₆ tetraether lipid-based proxy and a new correction for ocean bottom lipid overprinting

Jeremy N. Bentley^a, Gregory T. Ventura^a, Clifford C. Walters^b, Stefan M. Sievert^c, Jeffrey S. Seewald^c

^a Department of Geology, Saint Mary's University, Halifax, Nova Scotia B3H 3C3, Canada.

^b Bureau of Economic Geology, University of Texas at Austin, USA.

^c Woods Hole Oceanographic Institution, Woods Hole, USA.

* Corresponding author: Todd.ventura@smu.ca

For submission to: *Biogeosciences*

Number of pages: 3227

Number of Figures: 6

Number of Tables: 2

Supplementary pages: 6

Key Points

- High *i*GDGTs turnover in shallow sediments is shown to be non-selective and does not impact TEX₈₆ paleoclimate ratios.
- The proxy ~~nonetheless can be overprinted by addition of~~ can be overprinted by adding sediment sourced lipids when geothermal temperatures rise above ~60–70 °C.
- A universally applicable, diagenetic correction model is presented to remove overprinting artifacts in the TEX₈₆ proxy.

Abstract

The diversity and relative abundances of tetraether lipids produced by ~~Thaumarchaeota archaea and bacteria~~ in soils and sediments are increasingly ~~is are~~ used to assess environmental change. For instance, the TetraEther index of 86 carbon atoms (TEX₈₆), based on archaeal isoprenoidal glycerol dialkyl glycerol tetraether (*i*GDGT) lipids, is frequently applied to reconstruct past sea-surface temperatures (SST). Yet, it is unknown how the ratio fully responds to environmental and/or geochemical variations and if the produced signals are largely the adaptive response by Thaumarchaeota to ~~oceanographic effects associated with climate or seasonal driven~~ temperature changes in the upper water column. We present the results of a four push-core transect study of surface sediments collected along an environmental gradient at the Cathedral Hill hydrothermal vent system in Guaymas Basin, Gulf of California. The transect crosses a region where advecting hydrothermal fluids reach 155 °C within the upper 21 cm below the seafloor (cmbsf) close to the vent center to near ambient conditions at the vent periphery. The recovered *i*GDGTs closest to the vent center experienced high rates of turnover with up to 94% of the lipid pool being lost within the upper 21 cmbsf. Here, we show ~~that the turnover is non-selective across TEX₈₆ GDGT lipids and does not affect the ratio independently the turnover is non-selective across TEX₈₆ GDGT lipid classes and does not independently affect the ratio.~~ However, as evident by TEX₈₆ ratios being highly correlated to the Cathedral Hill vent sediment porewater temperatures ($R^2 = 0.84$), the ratio can be strongly impacted by the combination of severe lipid loss ~~when it is coupled to~~ with the addition of *in situ* *i*GDGT production from archaeal communities living in the vent sediments. – The resulting signal overprint produces absolute temperature offsets of up to 4 °C based on the TEX₈₆^H -calibration relative to modern climate records of the region. The overprint is also striking given the flux of GDGTs from the upper water column is estimated to

Commented [JB1]: l. 34: The sentence should be rephrased to read "...of tetraether lipids produced by archaea and bacteria in soils and sediments..." or something similar. Thaumarchaeal GDGT proxies are not readily applied to soil samples (I guess the idea here is a comparison with bacterial brGDGTs?).

Formatted: Subscript

Commented [JB2]: l. 45: the phrase "...across TEX₈₆ GDGT lipid classes" is confusing here since IPLs have not been introduced yet.

be ~93% of the combined intact polar lipid (IPL) and core GDGT lipid pool initially deposited on the seafloor. A model to correct the overprint signal using IPLs is therefore presented that can similarly be applied to all near-surface marine sediment systems where calibration models or climate reconstructions are made based on the TEX₈₆ measure.

1. Introduction

Archaeal and bacterial tetraether cellular membrane lipids represent a group of common and structurally diverse compounds frequently used to track the presence of living and dead microorganisms as well as geochemical and physical conditions within present-day and paleoenvironments (e.g., Schouten et al., 2002, 2004; 2013; Hopmans et al., 2004; Weijers et al., 2007, 2014; Hollis et al., 2012; O'Brien, et al., 2017; Stuart et al., 2017). In this regard, the proportional abundances of these lipids form various prominent proxies for assessing environmental change through time. For example, TEX₈₆ (TetraEther indeX with 86 carbon atoms; Schouten et al., 2002) is the most widely commonly used archaeal lipid-based paleotemperature proxy for marine environments (Table 1; Eq. 1). The ratio measures variations in the number of cyclopentyl rings for a select group of archaeal core lipids (CLs) (Supplementary Figure A-S1) following the assumption that biphytanyl cyclization is an organismal response to changing sea surface temperatures (SSTs). The proxy is therefore used in many different regions around the world with TEX₈₆ values typically ranging from 0.2–0.9 in marine settings (e.g. Huguet et al., 2006; Kim et al., 2008; McClymont et al., 2012; Tierney, 2014). with TEX₈₆ values typically ranging from 0.2–0.9 in both marine settings and lake sediment (Sinninghe-Damsté et al., 2009; Powers et al., 2010; Zhang et al., 2016; Morrissey et al., 2018; Yao et al., 2019; Kumar et al., 2019). The utility of TEX₈₆ rests on the premise that isoprenoidal GDGTs (iGDGTs) found in ocean bottom sediments are almost exclusively produced by marine planktonic archaea that inhabit the epipelagic zone (Wakeham et al., 2003; Tierney, 2014; Besseling Blessing et al., 2019, 2020). TEX₈₆-based lipids are therefore required to be efficiently and continually transported from the upper water column to the underlying ocean floor sediments to produce a chemostratigraphic record of microbial response to changing SST conditions with time (Wuchter et al., 2005).

Since its introduction, the reliability of TEX₈₆ to accurately track paleoclimate variations has been questioned. TEX₈₆-based SST estimates have been observed to substantially deviate from other temperature proxies (e.g., Huguet et al., 2006; Rommerskirchen et al., 2011; Seki et al., 2012). For example, over the past decade, considerable effort has been made to reconstruct the early Paleogene greenhouse climate system. However, TEX₈₆ appears to significantly over-estimate reconstructed SSTs (Hollis et al., 2012) relative to other proxies such as Mg/Ca, or clumped isotopic compositions of foraminiferal calcite, as well as various climate models based on partial pressure of carbon dioxide (pCO₂) predictions (Lunt et al., 2012; Naafs et al., 2018). For late Neogene climate reconstructions, the proxy has been shown to underestimate warming trends relative to the $-U_{37}^{K'}$ -alkenone-index derived temperatures (Lawrence et al., 2020). The apparent offsets in SST reconstructions have been attributed to complications arising from a lack of understanding on how the proxy's associated lipids change in relation to their environment and if these changes are regulated by internal adaptations within the archaeon or by an overarching community succession. In this regard, the debate surrounding these offsets largely centers on establishing responses to seasonal biases (e.g. Herford et al., 2006; Wuchter et al., 2006; Huguet et al., 2011); the development of adequate calibration methods (e.g. Kim et al., 2010; Pearson et al., 2013; Tierney et al., 2014); identifying lipid sourcing effects – including subsurface sediments origins for those used with the calculation of TEX₈₆ (e.g. Lipp and Hinrichs, 2009; Ho and Laepple, 2016); or as the result of physical, chemical, and ecological controls on archaeon iGDGTs cyclization (e.g. Elling et al., 2015; Qin et al., 2015; Hurley et al., 2016).

For the various non-thermal influences, the primary concern has been what archaeal taxa produce iGDGTs and where they are sourced. To this end, most TEX₈₆-based lipids are thought to be produced by Marine Group I (MGI) planktonic Thaumarchaeota (Brochier-Armanet et al., 2008), which are most abundant below the photic and epipelagic zone (e.g., Karner et al., 2001). Some inputs from Marine Group II (MGII), Euryarchaeota, that live in the upper 100 m of the water column, may also contribute to the sediment pool (Lincoln et al., 2014; Wang et al., 2015; Ma et al., 2020). Within this context, many regions of the ocean floor may become highly impacted by colder, deeper water column the collection of mixed source inputs

Commented [JB3]: l. 59: please specify “geochemical and physical conditions”.

Commented [JB4]: l. 64: the reference to Tab. 1 should probably be deleted here?

Commented [JB5]: l. 77: is there a reference that would support this statement?

Commented [JB6]: l. 92: Ho & Laepple (2016) do not discuss benthic production of GDGTs and there is substantial criticism of the 0-900m depth calibration suggested by these authors (see <https://doi.org/10.1038/ngeo2997>)

Commented [JB7]: l. 99-101: highly controversial.

Commented [JB8R7]:

from the colder, deeper water column. For example, a strong positive correlation was shown to exist between ocean depth and differences in TEX_{86}^H values for both surface sediments and suspended particulate organic matter in the Mediterranean Sea (Kim et al., 2015). Here TEX_{86} dissimilarities appear to be driven by increases in the relative abundances of the GDGT-2 and isomers of crenarchaeol (see Lui et al., 2018; Sinninghe Damsté et al., 2018) coupled ~~to-with~~ decreasing abundances of GDGT-1 and GDGT-3 ~~below the thermocline and the ammonium maxima within the deeper waters of the water column thereby producing to produce~~ a systematic reconstructed SST bias for deep-water surface sediments. Similar conditions have been observed for the Pacific Ocean (Karner et al., 2001; Pearson et al., 2013) and Southern Atlantic (Hurley et al., 2016) where peak archaeal abundances occur at 100–350 m depth. For these regions, the TEX_{86} lipids should not produce a direct response to changing SSTs. These sourcing effects have led to speculation that the TEX_{86} ratio of open ocean sediments may actually reflect deeper water column and subsurface rather than SSTs (Huguet et al., 2007; Lopes dos Santos et al., 2010; Kim et al., 2012a,b; Ho & Laepple, 2016; Hurley et al., 2016). To address this, Schouten et al. (2013) proposed a calibration based on suspended particulate matter and *in situ* water temperature from the upper 100 m of the global ocean. Both TEX_{86}^H and TEX_{86}^L (Kim et al., 2012a,b) have also been re-calibrated against subsurface (0–900 m water depth) temperatures ((Kim et al., 2012a,b; Ho & Laepple, 2016; Sinninghe Damsté?).

Other non-thermogenic driving forces impacting the production, cyclization, and relative abundance of TEX_{86} -based lipids include organismal selectivity to specific growth phases and growth rates (Elling et al., 2014; Hurley et al., 2016); redox conditions (Qin et al., 2015); and ~~by~~ the incorporation of *i*GDGT from archaeal communities living in the ocean floor sediments. With respect to the latter, Lipp and Hinrichs (2009) demonstrated that the production of intact polar lipid GDGTs (IPL-GDGTs) by ocean floor sediment microbial communities collected in the Peru Margin were distinctly different from upper water column sourced CLs and that the conversion of this living pool to fossil lipids would shift TEX_{86} ratios to higher values. However, ~~other authors have found TEX_{86} ratios are not impacted by benthic archaea due to the low relative turnover rates for the lipids in marine sediments.~~ Umoh et al. (2020) found little effect to the TEX_{86} paleoclimate ratio when examining surface sediments near hydrothermal vent sites on the Southeast Indian Ridge in the southern Indian Ocean. Lengger et al. (2012, 2014) reported no significant deviation between the TEX_{86} values in sediment cores collected near the oxygen minimum zone from that of the overlying water column in the Arabian Sea with near linear degradation rates of both IPLs and CLs. All together, the *i*GDGT relative abundances recorded in a sediment TEX_{86} measurement may ultimately constitute a multi-variable datapoint, mixing lipid components that are themselves responses to temperature, organismal substrate and metabolism dynamics, and biozone niche partitioning that spans from the ocean surface to *in situ* shallow sediment community pools lastly further attenuated by depositional and diagenetic processes.

While not an ideal location to create SST reconstructions, hydrothermal vents of sedimented ocean basins do represent an anomalous endmember to the vast expanse of ambient ocean floor sediment where paleoclimate reconstructions are commonly produced. ~~The Guaymas Basin, Gulf of California (Figure 1) is one such site as this location offers an ideal setting to compare TEX_{86} proxy responses to *in situ* lipid production from thermophilic sedimentary archaea, which differ from the pelagic background communities (e.g. Schouten et al., 2003). The Guaymas Basin, Gulf of California (Figure 1) is one such site.~~ The basin experiences ~~elevated-high~~ sedimentation rates ranging ~~between-from~~ 0.4–0.2 cm yr⁻¹ (Curry et al., 1979; Gieskes et al., 1988) due in part to the high productivity of the upper water column. The ocean floor hydrothermally impacted surface sediments are also a location of active and diverse microbial communities with vents that are often covered by Beggiatoa dominated microbial mats (e.g. McKay et al., 2012; Meyer et al., 2013; Teske et al., 2016). These sites should in principle, enable a high-resolution archaeal lipid stratigraphic record that provides optimal conditions for studying potential shallow diagenetic and subseafloor interferences to common archaeal lipid-based environmental proxies. ~~Recently~~Recently, Bentley et al. (2022) produced a survey of the source and diagenetic and catagenetic alteration of archaeal lipids from the Cathedral Hill hydrothermal vent complex (Figure 1) in the Guaymas Basin, Gulf of California. Within that investigation, it was observed that most *i*GDGTs were sourced from the overlying water column. ~~Building on the results of Schouten et al. (2003), it~~ was ~~also~~observed that these lipids can become heavily turned over in the hotter portions of the vent site where they rarely survive long enough to become cracked into hydrocarbon biomarkers such as biphytanes and derivatives of biphytanes. For this study, we further examine the *i*GDGT lipid distributions in these near-surface ocean floor sediments to determine if paleoclimate proxy signals can be impacted by the presence of subsurface archaeal

Commented [JB9]: reviewer wants this in? what year?

Commented [JB10]: l. 116: this sentence should be more specific, Kim et al. do not calibrate against 0-900m depth.

Commented [JB11]: l. 130-134: sentence could be split into two more digestible sentences.

Formatted: Subscript

Formatted: Font: Italic

Commented [JB12]: l. 139: “elevated sedimentation rates” in comparison to?

Commented [JB13]: L. 139-145. I challenge the notion that these two studies showed that *in situ* sedimentary production changed TEX_{86} values. In fact other studies (eg Lengger studies, Schouten et al., 2010) have shown that the IPLs in the study of eg Lips and Hinrichs are not derived from living Archaea but fossil IPLs because of the excellent preservation of pelagic glycosidic GDGTs (eg Xie et al., 2013, PNAS). This aspect should perhaps be more clear from the introduction, i.e. the simple presence of glycosidic GDGTs in sediments is in itself not proof of *in situ* sedimentary production.

populations. The distribution of *i*GDGTs and their corresponding environmental proxy signals were measured within the sediments along a transect at the complex. In this regard, this site offers the unique opportunity to evaluate the response of TEX₈₆ and other tetraether-lipid proxies within a microbially diverse sedimentary environment that is exposed to high temperature vent fluids.

Commented [JB14]:

1. 153-154: This sentence suggests that additional measurements were conducted for this study rather than specifically stating that the data from Bentley et al. (2022) are used.

L.162-181. The justification of using the Guaymas basin to determine in situ production is not only the active subsurface population but also that the GDGT fingerprint of these thermophilic sedimentary archaea is different from the pelagic background, as first established by Schouten et al. (2003) for this basin. Would be useful to clarify this here. If the distributions would have been similar, the signal would have likely been difficult to pick up.

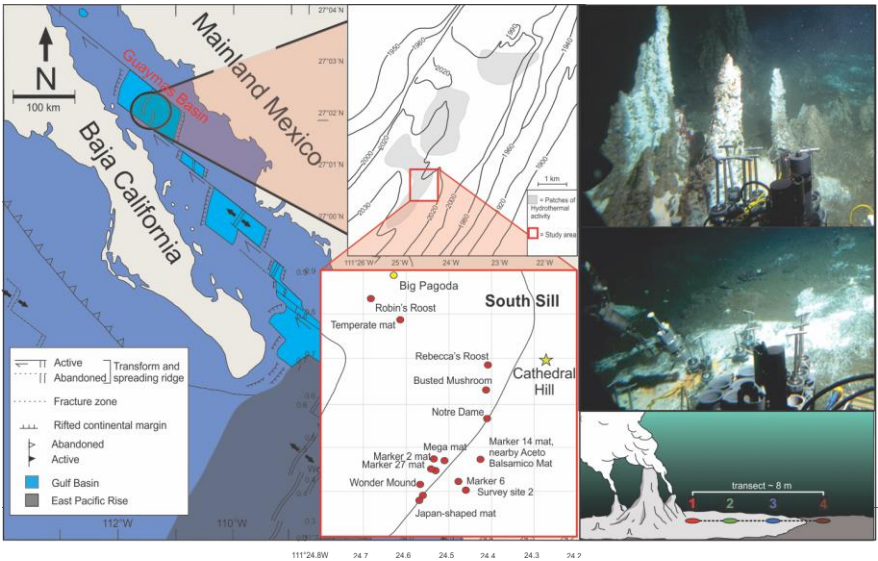


FIGURE 1 A) Location map of Guaymas Basin and the Southern Sill (red outlined box) in the Gulf of California. Cathedral Hill is marked with a yellow star. B) Photo of Cathedral Hill taken via *Alvin*. C) Schematic of the push core transect with a color-coding that is consistent for all plots throughout this paper. Maps modified from Teske et al. (2016), Dalzell et al. (2021), and Bentley et al. (2022).

2. Material and methods

2.1. Study location and sampling

Four sediment push cores were collected using HOV *Alvin* (Dive 4462; 10/22/08) at the Cathedral Hill hydrothermal vent site, located at a water depth of 1996 m in the Southern Trough of Guaymas Basin, Gulf of California (27°0.629' N, 111°24.265' W) (Figure 1). The push cores, labeled 1 to 4, were taken along a transect with ~ 2 m spacing extending outwards from microbial mat-covered sediments near the sulfide chimney complex to just outside of the microbial mat area in ambient seafloor sediment. Thermal-probe measurements were sequentially taken beside each core (Table 1). Once the push cores were brought to the surface, the sediments were subsampled into 2–3 cm-thick depth intervals, transferred to combusted glass vials, and immediately stored at -40 °C (onboard the ship) before being shipped under dry ice to the laboratory and later freeze-dried and stored at -80 °C.

191
192
193
194
195
196
197
198
199
200
201
202
203
204
205

Table 1. Sediment geochemical and lipid proxy data.

Core ^a	Depth interval (cmbsf)	Alvin dive # and core ID	Description/lithology ^b	Pore water temperature (°C) ^c	Interpolated Pore water temperature (°C) ^c	Sediment weight (g) ^{d,e}	TLE (mg g sed ⁻¹) ^e	Sum of IPL /GDGT ^f (μg g ⁻¹) ^e	St /C ^g (μg g ⁻¹) ^e
1	0-2	GB4462-5	Black mud with microbial mat filaments	19	19	1.97	11.5	16.7	1.7
1	2-4	GB4462-5	Brownish-green diatomaceous mud	-	67	2.04	7.65	14.6	1.4
1	4-6	GB4462-5	Brownish-green diatomaceous mud	85	85	2.03	9.37	6.0	4.3
1	6-8	GB4462-5	Brownish-green diatomaceous mud	-	105	1.99	2.09	4.3	3.2
1	8-10	GB4462-5	Brownish-green diatomaceous mud	-	117	2.01	4.38	3.2	1.7
1	10-12	GB4462-5	Grayish-green mud	121, 124	125	2.01	1.97	1.7	1.4
1	12-15	GB4462-5	Brownish-green consolidated mud with clay shards	-	135	1.98	1.99	1.4	0.0
1	15-18	GB4462-5	Brownish-green consolidated clay	142	145	1.96	1.69	0.0	0.0
1	18-21	GB4462-5	Brownish-green consolidated clay	153	153	1.98	1.72	0.0	0.0
2	0-2	GB4462-6	Black mud with microbial mat filaments	9, 13	11	2.02	8.48	17.8	7.5
2	2-4	GB4462-6	Black mud with microbial mat filaments	-	22	1.97	8.65	7.5	2.5
2	4-6	GB4462-6	Brownish-green diatomaceous mud	20	20	1.95	2.51	2.5	3.4
2	6-8	GB4462-6	Brownish-green diatomaceous mud	-	47	1.95	3.38	3.4	2.0
2	8-10	GB4462-6	Brownish-green diatomaceous mud	-	60	1.95	1.48	2.0	1.0
2	10-12	GB4462-6	Brownish-green diatomaceous mud	69, 77	73	1.94	4.19	2.0	0.0
2	12-15	GB4462-6	Brownish-green diatomaceous mud	-	87	2.02	1.69	1.0	0.0
2	15-18	GB4462-6	Brownish-green diatomaceous mud	118	105	1.95	2.01	0.0	0.0
2	18-21	GB4462-6	Brownish-green diatomaceous mud	109	125	1.94	1.38	0.0	0.0
3	0-2	GB4462-3	Black mud with microbial mat filaments	3.2	3.2	1.96	7.31	15.3	8.3
3	2-4	GB4462-3	Brownish-green diatomaceous mud	-	8	1.96	3.91	8.3	7.0
3	4-6	GB4462-3	Brownish-green diatomaceous mud	15	15	2.00	2.86	7.0	5.7
3	6-8	GB4462-3	Brownish-green diatomaceous mud	-	26	2.02	5.00	5.7	5.8
3	8-10	GB4462-3	Brownish-green diatomaceous mud	34	34	1.97	2.02	5.7	6.5
3	10-12	GB4462-3	Brownish-green diatomaceous mud	-	43	2.01	1.86	5.8	12.3
3	12-15	GB4462-3	Brownish-green diatomaceous mud	-	54	1.94	1.78	6.5	5.2
3	15-18	GB4462-3	Brownish-green diatomaceous mud	61	66	2.01	1.43	12.3	16.7
3	18-21	GB4462-3	Brownish-green diatomaceous mud	83	80	1.96	1.98	5.2	14.6
4	0-2	GB4462-8	Black mud	0	0	1.93	3.44	16.7	6.0
4	2-4	GB4462-8	Brownish-green diatomaceous mud	1.5	8	2.01	3.17	14.6	4.3
4	4-6	GB4462-8	Brownish-green diatomaceous mud	16	16	1.95	4.00	6.0	3.2
4	6-8	GB4462-8	Brownish-green diatomaceous mud	-	18	2.02	4.19	4.3	1.7
4	8-10	GB4462-8	Brownish-green diatomaceous mud	-	21	2.02	4.76	3.2	1.4
4	10-12	GB4462-8	Brownish-green diatomaceous mud	-	23	1.95	4.84	1.7	0.0
4	12-15	GB4462-8	Brownish-green diatomaceous mud	-	25	1.95	5.74	1.4	0.0
4	15-18	GB4462-8	Sample lost during collection	-	-	-	-	0.0	0.0
4	18-21	GB4462-8	Sample lost during collection	29	-	-	-	0.0	0.0

206
207
208
209
210
211
212
213
214

Table 1. Sediment geochemical and lipid proxy data (continued).

Core ^a	Depth interval (cmbsf)	Alvin dive # and core ID	SUM of TEX ₈₆ cGDGT ^c (μg g ⁻¹)	TEX ₈₆ fGDGT ^c	TEX ₈₆ ^H Core cGDGT ^d	TEX ₈₆ ^H Recon structured SSTs (Kim et al., 2010) ^e	RI ^f	MI ^g	TEX ₈₆ fGDGT ^c	TEX ₈₆ Core cGDGT ^c
1	0-2	GB4462-5	110.7	0.56	-0.25	21.2	2.44	0.34	0.58	0.56
1	2-4	GB4462-5	117.1	0.58	-0.23	22.6	2.45	0.38	0.58	0.58
1	4-6	GB4462-5	47.7	0.58	-0.24	22.3	2.48	0.36	0.55	0.58
1	6-8	GB4462-5	33.0	0.58	-0.24	22.2	2.55	0.35	0.57	0.58
1	8-10	GB4462-5	13.0	0.59	-0.23	22.9	2.60	0.34	0.72	0.59
1	10-12	GB4462-5	10.1	0.57	-0.25	21.8	2.63	0.31	0.70	0.57
1	12-15	GB4462-5	17.8	0.61	-0.22	23.8	2.65	0.37	0.69	0.61
1	15-18	GB4462-5	9.8	0.61	-0.22	23.9	2.66	0.36	-	0.61
1	18-21	GB4462-5	9.3	0.63	-0.20	24.9	2.66	0.38	-	0.63
2	0-2	GB4462-6	128.5	0.55	-0.26	20.6	2.52	0.32	0.46	0.55
2	2-4	GB4462-6	58.2	0.54	-0.27	20.4	2.52	0.32	0.58	0.54
2	4-6	GB4462-6	19.2	0.54	-0.27	20.4	2.53	0.33	0.60	0.54
2	6-8	GB4462-6	13.4	0.56	-0.25	21.5	2.68	0.29	0.71	0.56
2	8-10	GB4462-6	9.3	0.58	-0.25	21.7	2.70	0.29	0.70	0.58
2	10-12	GB4462-6	10.1	0.57	-0.24	21.9	2.71	0.28	0.68	0.57
2	12-15	GB4462-6	8.5	0.57	-0.24	21.9	2.73	0.28	0.73	0.57
2	15-18	GB4462-6	4.5	0.58	-0.23	22.6	2.68	0.31	-	0.58
2	18-21	GB4462-6	6.0	0.59	-0.23	22.8	2.74	0.28	-	0.59
3	0-2	GB4462-3	127.0	0.54	-0.27	20.2	2.41	0.37	0.53	0.54
3	2-4	GB4462-3	57.7	0.53	-0.27	19.8	2.62	0.27	0.49	0.53
3	4-6	GB4462-3	60.0	0.53	-0.27	19.9	2.53	0.31	0.56	0.53
3	6-8	GB4462-3	59.8	0.54	-0.27	20.3	2.50	0.33	0.54	0.54
3	8-10	GB4462-3	53.0	0.53	-0.27	19.9	2.54	0.31	0.61	0.53
3	10-12	GB4462-3	42.1	0.54	-0.27	20.3	2.64	0.27	0.74	0.54
3	12-15	GB4462-3	39.2	0.56	-0.25	21.5	2.56	0.30	0.69	0.56
3	15-18	GB4462-3	86.8	0.55	-0.26	20.9	2.77	0.26	0.74	0.55
3	18-21	GB4462-3	36.4	0.57	-0.25	21.6	2.68	0.29	0.66	0.57
4	0-2	GB4462-8	112.9	0.54	-0.27	20.4	2.43	0.35	0.54	0.54
4	2-4	GB4462-8	85.3	0.53	-0.27	20.0	2.59	0.30	0.37	0.53
4	4-6	GB4462-8	102.7	0.54	-0.27	20.2	2.55	0.31	0.43	0.54
4	6-8	GB4462-8	70.8	0.52	-0.28	19.3	2.55	0.29	0.45	0.52
4	8-10	GB4462-8	26.6	0.53	-0.27	19.9	2.69	0.26	-	0.53
4	10-12	GB4462-8	91.0	0.53	-0.27	19.8	2.54	0.30	-	0.53
4	12-15	GB4462-8	73.7	0.53	-0.28	19.7	2.90	0.20	-	0.53
4	15-18	GB4462-8	110.7	-	-	-	-	-	-	-
4	18-21	GB4462-8	117.1	-	-	-	-	-	-	-

^a As also reported in Bentley et al. (2022).

^c Sum of GDGT-1, -2, -3, -4, -5, and -5' (Table S1).

^d Sum of all detected 1G- and 2G-GDGTs (Table S3).

^a Collected core numbers are relabelled in the sample name to reflect a relative transect position (1-4).

^b Sediment lithology based on freeze-dried sediments.

^c TEX₈₆ = (GDGT-2 + GDGT-3 + GDGT-5')/(GDGT-1 + GDGT-2 + GDGT-3 + GDGT-5'), (Schouten et al., 2002) applied to both core GDGTs and 1-glycosyl-GDGTs.

^d TEX₈₆^H = log ((GDGT-2 + GDGT-3 + GDGT-5')/(GDGT-1 + GDGT-2 + GDGT-3 + GDGT-5')), for sediments outside the polar regions/low latitudes (Kim et al., 2010).

^e Following the mean annual sea surface calibration of 0 m water depth (SST = 68.4 × TEX₈₆^H + 38.6) of Kim et al. (2010).

^f Ring index (RI) = 0×(GDGT-0) + 1×(GDGT-1) + 2×(GDGT-2) + 3×(GDGT-3) + 4×(GDGT-4) + 5×(GDGT-5)/ΣGDGTs, adapted from Pearson et al. (2004) and promoted by Zeng et al. (2016).

[§] Methane index (MI) = (GDGT-1 + GDGT-2 + GDGT-3)/(GDGT-1 + GDGT-2 + GDGT-3 + GDGT-5 + GDGT-5') by Zhang et al. (2011).

2.2. Lipid extraction

Lipid extractions followed a modified Bligh and Dyer protocol laid out in Bentley et al. (2022) and following Sturt et al. (2004). A subsample of freeze-dried sediment was added to a Teflon[®] centrifuge tube followed by the addition of 6 ml of mix A solvent solution comprising of 2:1:0.8 v/v/v methanol (MeOH), dichloromethane (DCM), and phosphate buffer (5.5 g L⁻¹ Na₂HPO₄; Avantor Performance Materials, LLC, adjusted to pH of 7.4 with HCl; Anachemia Co.). The solvent sediment mixture was further spiked with 1-alkyl-2-acetoxy-*sn*-glycero-3-phosphocholine (PAF) recovery standard purchased from Avanti Polar Lipids, Inc. The slurry was sonicated for 5 min then centrifuged for 5 min at 1250 rpm. The resulting supernatant was added to a separatory funnel. This procedure was performed twice before being joined by two replicate extractions using mix B, a 2:1:0.8; v/v/v solution of MeOH, DCM, and trichloroacetic acid buffer (50 g L⁻¹ C₂HCl₃O₂; Avantor Performance Materials, LLC, of pH 2) and a final two replicate extractions using mix C, a 5:1 v/v solution of MeOH and DCM. Once complete, the combined A, B, and C. For each step, the organic fraction was collected in a beaker, and the combination of mix A, B, and C were subjected to 10 ml of DCM and H₂O (MilliQ) to achieve separation. The organic phase was drawn off and the water was extracted using 3 DCM washes, drawing off the organic phase after each wash. The organic phase was then back-extracted with H₂O to ensure purity. The resulting organic phase was then evaporated to dryness at 60 °C under dry nitrogen. The resulting total lipid extract (TLE) was transferred to pre-weighed autosampler vials using DCM:MeOH 1:1 v/v, spiked with 1, 2-diheneicosanoyl-*sn*-glycero-3-phosphocholine (C₂₁-PC; Avanti Polar Lipids, Inc.) and stored at -20 °C.

2.3. High performance liquid chromatography – mass spectrometry (HPLC-MS)

Mass spectrometric analyses were performed on an Agilent Technologies 1260 Infinity II HPLC coupled to an Agilent Technologies 6530 quadrupole time-of-flight mass spectrometer (qToF-MS) operated in positive mode. Chromatographic separation used a reverse-phase method outlined by Zhu et al. (2013). The HPLC was fitted with an Agilent Technologies ZORBAX RRHD Eclipse Plus C₁₈ (2.1 mm × 150 mm × 1.8 μm) reverse phase column and guard column maintained at 45 °C. The sample injection solvent was methanol. An aliquot of each sample representing 1% of the TLE was analyzed. A 0.25 mL min⁻¹ flow rate was established with mobile phase A consisting of methanol/formic acid/ammonium hydroxide (100:0.04:0.10 v/v/v) held at 100% for 10 min, thereafter mixed following a linear gradient with mobile phase B (propan-2-ol/formic acid/ammonium hydroxide (100:0.04:0.10 v/v/v) to 24%, 65%, and 70% over 5-, 75-, and 15-min intervals, respectively. Each sample run was finished by re-equilibrating the system with 100% mobile phase A for 15 min. The effluent was ionized by an electrospray ionization source with a gas temperature of 300 °C, a 3 L min⁻¹ drying gas flow, and a 5.33 μA source current. The mass spectrometer was set to a 100–3000 *m/z* scan range in positive mode in an untargeted method with 10 ppb resolution to simultaneously resolve both archaeal IPLs and CLs.

Analyte identification was achieved by accurate mass resolution, mass spectral analysis using Agilent Technology's MassHunter software, and comparison of fragmentation patterns with the literature (e.g., Knappy et al., 2009; Liu et al., 2010; Yoshinaga et al., 2011 – see Bentley et al., 2022 for further details). Mass fragments consistent with the loss of a biphytane (*m/z* 743.7) were screened for all archaeal lipids. Quantification was achieved by summing the integration peak areas of [M+H]⁺, [M+NH₄]⁺, and [M+Na]⁺ adducts for the respective IPLs and CLs of interest. Concentration values were obtained relative to the internal C₂₁-PC standard and reported in μg/g dry sediment weight. Response factors were determined by a series of injections of a standard solution containing: PAF, C₂₁-PC, 1,2-diacyl-3-O-(α-D-galactosyl)-β-D-galactosyl-*sn*-glycerol (DGDG), 1,2-diacyl-3-O-β-D-galactosyl-*sn*-glycerol (MGDG), 1,2-di-O-phytanoyl-*sn*-glycerol (Archaeol), 1',3'-bis[1,2-dimyristoyl-*sn*-glycero-3-phospho]-glycerol (14:0 Cardiolipin) from Avanti Polar Lipids, Inc., USA, and 2,2'-di-O-decyl-3,3'-di-O-(1'',ω''-eicosanoyl)-1,1'-di-(rac-glycerol) (C₄₆-GTGT) from Pandion Laboratories, LLC in amounts ranging from 100 pg to 30 ng. Response factors

Formatted: Superscript

Commented [JB15]: 1. 255-256: which mode was used? Targeted/untargeted? And what is the resolution of the Q-ToF?

Commented [JB16R15]: I feel like this is unnecessary, I never see this information in other papers

291 were calculated relative to the C₂₁-PC, and the appropriate correction factor was then applied to the lipid
292 class of interest.

293
294 A series of samples were re-run to identify or confirm deviations in the data set. The variations between the
295 concentrations of GDGTs in the re-run and the initial runs yielded a maximum difference of $\sim \pm 4 \mu\text{g g}^{-1}$ per
296 GDGT compound, providing confidence in the initial results and confirming the presence of two outliers in
297 the data set (Bentley et al., 2022). These outliers are Core 4 at 8-10 cm, with abnormally low concentrations
298 of all compounds that are likely ion suppression from a sample heavily impregnated with oil, and Core 3 at
299 15-18 cm, which contains relatively high lipid concentrations that are yet to be explained.

2.2. Lipid extraction

301 Lipid extractions followed a modified Bligh and Dyer protocol laid out in Bentley et al. (2022) and
302 following Sturt et al., 2004. A subsample of freeze-dried sediment was added to a Teflon[®] centrifuge tube
303 followed by the addition of 6 mL of mix A solvent solution comprising of 2:1:0.8 v/v/v methanol (MeOH),
304 dichloromethane (DCM), and phosphate buffer (5.5 g L⁻¹ Na₂HPO₄; Avantor Performance Materials, LLC;
305 adjusted to pH of 7.4 with HCl; Anachemia Co.). The solvent sediment mixture was further spiked with 1-
306 alkyl-2-acetyl-sn-glycerol-3-phosphocholine (PAF) recovery standard purchased from Avanti Polar Lipids,
307 Inc. The slurry was sonicated for 5 min then centrifuged for 5 min at 1250 rpm. The resulting supernatant
308 was added to a separatory funnel. This procedure was performed twice before being joined by two replicate
309 extractions using mix B, a 2:1:0.8; v/v/v solution of MeOH, DCM, and trichloroacetic acid buffer (50 g/L
310 C₂HCl₃O₂; Avantor Performance Materials, LLC, of pH 2) and a final two replicate extractions using mix C,
311 a 5:1 v/v solution of MeOH and DCM. Once complete, the combined A, B, and C mixed extracts were back
312 extracted in the separatory funnel by washing the organic phase with 1:1 v/v milliQ water and DCM,
313 followed by 6 additional washes (×3 with DCM followed by ×3 milliQ water washes). For each step, the
314 organic fraction was collected in a beaker and evaporated to dryness at 60 °C under a gentle stream of dry
315 nitrogen. The resulting total lipid extract (TLE) was transferred to preweighed autosampler vials using
316 DCM:MeOH 9:9 v/v, spiked with 1, 2-diheneicosanoyl-sn-glycerol-3-phosphocholine (C₂₁-PC; Avanti Polar
317 Lipids, Inc.) and stored at -20 °C.

2.3. High performance liquid chromatography—mass spectrometry (HPLC-MS)

322 Mass spectrometric analyses were performed on an Agilent Technologies 1260 Infinity II HPLC coupled to
323 an Agilent Technologies 6530 quadrupole time-of-flight mass spectrometer (qToF-MS) operated in positive
324 mode. Chromatographic separation used a reverse phase method outlined by Zhu et al. (2013). The HPLC
325 was fitted with an Agilent Technologies ZORBAX RRHD Eclipse Plus C₁₈ (2.1 mm × 150 mm × 1.8 μm)
326 reverse phase column and guard column maintained at 45 °C. Sample The sample injection solvent was
327 methanol. An aliquot of each sample representing 1% of the TLE was analyzed. A 0.25 mL min⁻¹ flow rate
328 was established with mobile phase A consisting of methanol/formic acid/ammonium hydroxide
329 (100:0.04:0.10 v/v/v) held at 100% for 10 min, thereafter mixed following a linear gradient with mobile
330 phase B (propan-2-ol/formic acid/ammonium hydroxide (100:0.04:0.10 v/v/v) to 24%, 65%, and 70% over
331 5, 75, and 15 min intervals, respectively. Each sample run was finished by re-equilibrating the system with
332 100% mobile phase A for 15 min. The effluent was ionized by an electrospray ionization source with a gas
333 temperature of 300 °C, a 3 L min⁻¹ drying gas flow, and a 5.33 μA source current. The mass spectrometer
334 was set to a 100–3000 m/z scan range to simultaneously resolve both archaeal IPLs and CLs.

336 Analyte identification was achieved by accurate mass resolution, mass spectral analysis using Agilent
337 Technology's MassHunter software and by comparison of fragmentation patterns with the literature (e.g.,
338 Knappy et al., 2009; Liu et al., 2010; Yoshinaga et al., 2011 — see Bentley et al., 2022 for further details).
339 Mass fragments consistent with the loss of a biphytane (m/z 743.7) were screened for all archaeal lipids.
340 Quantification was achieved by summing the integration peak areas of [M+H]⁺, [M+NH₄]⁺, and [M+Na]⁺
341 adducts for the respective IPLs and CLs of interest. Concentration values were obtained relative to the
342 internal C₂₁-PC standard and reported in μg/g dry sediment weight. Response factors were determined by a
343 series of injections of a standard solution containing: PAF, C₂₁-PC, 1,2-diacetyl-3-O-(α-D-galactosyl-1,6)-β-
344 D-galactosyl-sn-glycerol (DGDG), 1,2-diacetyl-3-O-β-D-galactosyl-sn-glycerol (MGDG), 1,2-di-O-phytanyl-
345 sn-glycerol (Archaeol), 1',3'-bis[1,2-dimyrystoyl-sn-glycerol-3-phospho]-glycerol (14:0 Cardiolipin) from

Commented [JB17]: l. 274: please express the reproducibility in %. Given that many GDGTs or IPLs have concentrations below 1 μg/g sediment (Tab. S1 and S2), the absolute deviation is not informative (there are few IPLs that occur at >4 μg/g).

Commented [JB18R17]: I'm not sure exactly what needs to be done here

Commented [JB19]: l. 235: why would MilliQ water be used for the final 3 "washes", if the mixture is not liquid-liquid extracted again?

Commented [JB20R19]: I don't understand this comment

Commented [JB21]: I'll need to adjust this section a bit.

Commented [JB22]: l. 255-256: which mode was used? Targeted/untargeted? And what is the resolution of the Q-ToF?

Commented [JB23R22]: I feel like this is unnecessary, I never see this information in other papers

A series of samples were re-run to identify or confirm deviations in the data set. The variations between the concentrations of GDGTs in the re-run and the initial runs yielded a maximum difference of $\sim \pm 4 \mu\text{g g}^{-1}$ per GDGT compound, providing confidence in the initial results and confirming the presence of two outliers in the data set (Bentley et al., 2022). These outliers are Core 4 at 8–10 cm, with abnormally low concentrations of all compounds that is likely ion suppression from a sample heavily impregnated with oil, and Core 3 at 15–18 cm, which contains relatively high lipid concentrations that are yet to be explained.

3. Results and Discussion

3.1. Archaeal lipid diversity and heterotrophic loss turnover

The Cathedral Hill transect sediments have *i*GDGTs containing 0–4 cyclopentyl (GDGT 0–4) as well as crenarchaeol (Cren) and the isomer of crenarchaeol (Cren') that contains five rings (four cyclopentyl and one cyclohexyl moiety) (Table S1). Branched GDGTs include including 4a-c, 2a11a-c, and 3a-111a were found to have discontinuous and/or low absolute abundances, with some compound classes not being detected (i.e. *br*GDGT-3b111b; Table S2). The *br*GDGTs are therefore not further examined in this study. For cores 1 to 3 the concentrations of nearly all *i*GDGT compounds systematically decrease with depth (Figure 2). Bentley et al. (2022) established the sedimentation of archaeal lipids from the upper water column as being uniform both in terms of spatial loading across the length of the transect as well as over the pastan inferred 52.5–105 yrs of sedimentation as penetrated by the length of the push core (based on sedimentation rates). From this, it is estimated that $\sim 70.57 \pm 23.5 \mu\text{g iGDGTs g}^{-1}\text{-sed yr}^{-1}$ is being deposited on the seafloor from the overlying water column. However, for cores closest to the vent site, lipid abundances exhibited a much sharper decrease with depth, which Bentley et al. (2022) attribute to the turnover of archaeal lipids coupled to, but not directly caused by, hydrothermalism. For cores 1 and 2, losses reach as high as 94% within the upper 21 cmbsf (cm below sea floor/seafloor). The lipid loss is less severe for core 3 at $\sim 60\%$. For the ambient core 4, *i*GDGTs have similar down core stratigraphic trends with a near-consistent average of $400 \mu\text{g g}^{-1}$ sediment concentration and no systematic loss of lipids.

Due to the extreme-high temperature conditions of the vent fluids conditions at Cathedral Hill, the identified archaeal *i*GDGT-based IPLs within the sediments most likely represent the composition of cellular membrane material from archaeal communities living in the sediments. These lipids have exclusively monoglycosyl (1G) or diglycosyl (2G) head groups linked to a 2,3-sn-glycerol. Within the pyrolytic environment, the transformation of IPL *i*GDGTs could hypothetically add to the core *i*GDGT lipid pool. Similar to CLs, the 1G-GDGTs range from 0 to -4 and include Cren and Cren'. Surface concentrations of these lipids are $\sim 15 \mu\text{g g}^{-1}\text{-sed}$ in cores 1 to 3 (residing within the microbial mat) and $11 \mu\text{g g}^{-1}\text{-sed}$ for core 4 (Table S2). Also similar to the CLs, the archaeal IPL concentrations decrease down core and are tightly controlled closely coupled to increasing by porewater temperatures (Table S2). For cores 1 and 2, the maximum depths for detectable 1G-GDGTs are 15–18 and 12–15 cmbsf, corresponding to vent porewater temperatures of 145 and 87 °C, respectively. In core 3, 1G-GDGTs persist down core with a consistent lipid depletion that reaches its lowest concentration of $5.22 \mu\text{g g}^{-1}\text{-sed}$ in the bottom of the core at 18–21 cmbsf sediment depth where porewater temperatures rise to 80 °C. In core 4, which is most similar to the ambient ocean bottom conditions and falls outside of the area covered by the microbial mat, the lipid concentrations average is $\sim 8 \mu\text{g g}^{-1}\text{-sed}$ across the depth of the core. The 2G-GDGTs have 0 to 2 cyclopentyl rings that for cores 1 and 2 are restricted to the upper 4 to 6 cmbsf. These lipids are not further investigated in this study as 2G-GDGTs are of limited abundance (max summed concentrations $< 7 \mu\text{g g}^{-1}\text{-sed}$) and their structural diversities negligibly effect-affect isoprenoid-based proxies.

Lipid-based proxies for the calibration or reconstruction of paleoclimate records such as TEX₈₆, BIT, CBT, and MBT, are based on environmentally scaled loadings-contributions of select GDGT compound-classes. These proxies could be negatively impacted should other ocean floor sediment systems experience high rates of lipid turnover (Lengger et al., 2014). To evaluate whether down-core depletions of lipid concentrations impacted tetraether-based proxies, the concentrations of the highly abundant GDGT-0 was plotted relative to the TEX₈₆ ratio lipids (*i*GDGT-1, -2, -3, and Cren') (Figure 3A). For figure 3A, straight

Commented [JB26]: 1. 282: heterotrophic loss is not addressed in this section.

Commented [JB27]:

Commented [JB28]: 1. 287-288: in Fig. 2, the concentrations in core 3 do not decrease systematically.

Commented [JB29]: Outliers? Does this mean they want us to write about the outliers in core 3 and 4

Formatted: Superscript

Commented [JB30]: 1. 299: specify “extreme vent fluid conditions”

Commented [JB31]: 1. 303: maybe rather “contain 0-4 cyclopentyl moieties...”

Commented [JB32R31]: What does this even mean???

Commented [JB33]: 1. 306: please add regression/correlation coefficient (or other statistical means) to demonstrate the “tight control” of porewater temperature.

lines in the logarithmic plot indicate near-equal depletion rates between the paired x- and y-axis lipid classes. Similarly, parallel parallel lines slopes for the various lipid pairs also indicates near-equal depletion rates, with vertical offsets between pairs marking different initial starting abundances of the compared lipid class. In this regard, iGDGT-0, -1, -2, and Cren' have undergone the same rate of turnover. However, the depletion rate of iGDGT-3's is lower than that of other lipid classes for cores 1 and 2. Although, this may represent a distinct resilience to turnover, we suggest it instead results from overprinting by the subsurface hyperthermophilic archaeal community (see below).

To better track changes across each core, the degradation rate constants (k') of TEX₈₆ lipid classes were calculated for each push core (Figure A2; Table A3) using a first-order kinetic model:

$$C_t = C_i \cdot e^{-k't} \quad (51)$$

in which C_t and C_i are concentration at time (t) and the initial concentration, respectively (e.g. Schouten et al., 2010). Rearranging Eq. 51, the k' were calculated as

$$k' = (-\ln[C_t/C_i])/t \quad (62)$$

From these data, it is evident that the down core concentrations of each lipid decrease at equivalent rates (i.e. they have the same slopes for their rates of decay $s^2 = 0.2$), the exception to this is for all but core 2, (i.e. they have the same slopes for their rates of decay, which independent of two outliers has different decay paths for GDGT-3 and GDGT-5, (m_{reg} = 0.2). This is consistent with the TEX₈₆ iGDGT lipid classes largely being removed from the sediment lipid pool in a non-selective manner.

Based on these results, the TEX₈₆, iRing index (RI), and mMethane index (MI) values were plotted against their respective summed iGDGTs lipid concentrations (Fig 3B–D). For samples located within the habitable zone (having porewaters ranging from 0–123 °C; Kashefi and Lovley, 2003), no correlation is observed between the lipid abundances and proxy ratios of TEX₈₆, RI, or MI (Figure 3B–D). This further suggests these proxies are not affected by turnover in the habitable zone. However, once sediment burial reaches beyond the habitable zone, TEX₈₆ ratios trend to higher values (similarly also reflected in GDGT-3 concentration trends of Figure 3A). Collectively, these data strongly indicate that archaeal lipid turnover is largely nonselective of the TEX₈₆ lipid classes and will therefore theoretically not in and of themselves significantly impact archaeal lipid paleoclimate proxy reconstructions.

Apart from paleoclimate reconstructions, archaeal lipid CLs are sometimes used to resolve aspects of localized biogeochemical cycles within sediments. To this end, the location and degree of anaerobic oxidation of methane (AOM) is determined by methane and archaeal lipid carbon² isotope measures (e.g. Boetius et al., 2000; Schouten et al., 2003; Stadnitskaia et al., 2008; Biddle et al., 2012) as well as by the proportional abundances of core GDGTs (cGDGTs) in the form of the methane index MI (MI; Zhang et al., 2011; Carretal., 2018; Petrick et al., 2019). With respect to the latter, the MI proxy is used to differentiate regions of normal marine (with values between 0–0.3) and active AOM conditions in an around cold seeps (where values >0.5–1 are reported for gas hydrate impacted sediments and subsurface environments with high AOM levels). To our knowledge, the use of this proxy for hydrothermal vent systems has not been thoroughly investigated even though this microbial process has been well documented at Guaymas Basin. For example, highly ¹³C-depleted CLs reaching up to -70‰ in hydrothermal vent sediments with porewater temperatures as high as 95 °C indicates thermophilic archaea actively engaging in AOM (Schouten et al., 2003). Biddle et al. (2012) through the detection of relevant archaeal communities by 16S RNA in conjunction with highly depleted methane carbon isotope values determined active AOM spanning 35 to 90 °C pore water conditions. AOM is not likely to be the dominant form of carbon and sulfur metabolism as it generally accounts for less than 5% of sulfate reduction (Kallmeyer and Boetius, 2004). When applying the MI to the Cathedral Hill push core transect survey very-low values (ranging from 0.2–0.38; Table 1) are recorded with no correspondence to thermal controls across the vent transect (Figure 4). Although, it could be considered that the low values arises from a lack of AOM within these sediments the low MI values are consistent with a high upper water column iGDGTs loading as estimated by Bentley et al. (2022).

Commented [JB34]: L. 318-324. Would be useful to mention the estimates of degradation of GDGTs of Schouten et al.

(2003) here for the same site: they actually found a difference between crenarchaeol versus other GDGTs. Indeed, what I am struck by is that the drastic change in GDGT distribution of GDGTs in Guaymas basin, in particular the dominance of GDGT4 with high temperatures, of Schouten et al. 2003 is not observed here. GDGT4 may co-elute with crenarchaeol under your UHPLC conditions so only mass spectra can distinguish the two. I presume this was done and also that if there was a coelution that the amount of GDGT-4 was corrected for the contribution of the [M+2+H]⁺ ion of crenarchaeol. Can you speculate why there is this difference between the two studies?

1. 317-320: BIT, CBT, MBT not introduced yet. Overall, these two sentences have very limited meaning, please be more specific. Which paleoclimate records (these proxies are used for different purposes), what is "environmentally scaled loading" (which parameters), what are "other ocean floor sediment systems" (this could mean anything from lateral influx to benthic production, I guess)?

Commented [JB35]: 1. 332: there seems to be something wrong with the numbering of the equations throughout the text.

Formatted: Superscript

Commented [JB36]: 1. 339-341: it would be helpful to quickly summarize the results here/provide some statistical analysis, so the reader can follow the argument made.

Commented [JB37]: 1. 346-347: this trend is primarily driven by the TEX₈₆ values obtained for core 1 whereas core 2 displays TEX₈₆ values mostly in agreement with the values determined for the habitable zone. It would be nice to see th

Commented [JB38]: 1. 353-354: please be more specific, which isotope systems?

Commented [JB39]: 1. 358: MI has been used in other than cold seep systems as well. Somewhere in this paragraph, it should be mentioned that contributions from Euryarchaeota are implied in such high-MI settings.

Formatted: Font: Italic

Commented [JB40]: 1. 367-369: I would not define 0.2-0.38 as "very low" values. How is any thermal control tested, please be more specific (include simple statistical analysis such as regression/correlation coefficients).

Commented [JB41R40]: Is this the comment?

Commented [JB42]: 1. 366: please be more specific, sulfate reduction rates?

Commented [JB43]: 1. 367-369: I would not define 0.2-0.38 as "very low" values. How is any thermal control tested, please be more specific (include simple statistical analysis such as regression/correlation coefficients).

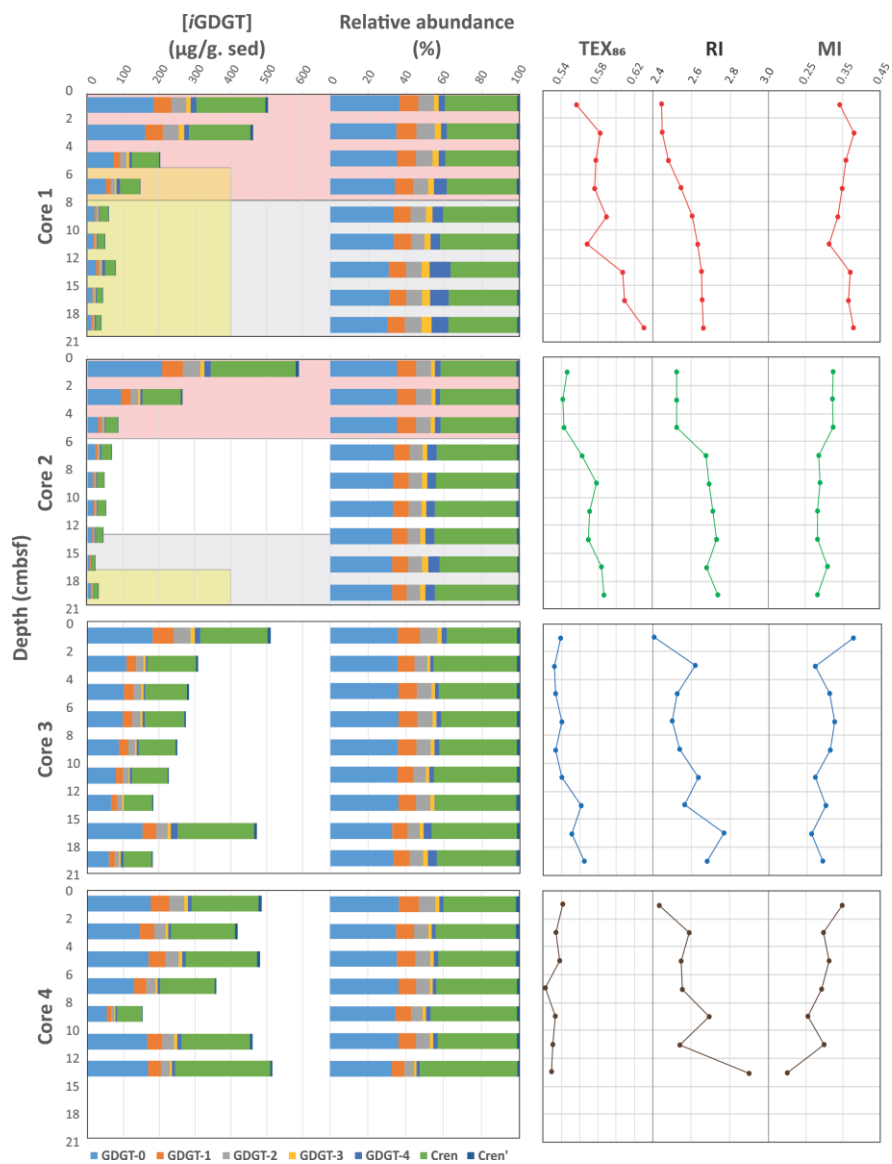
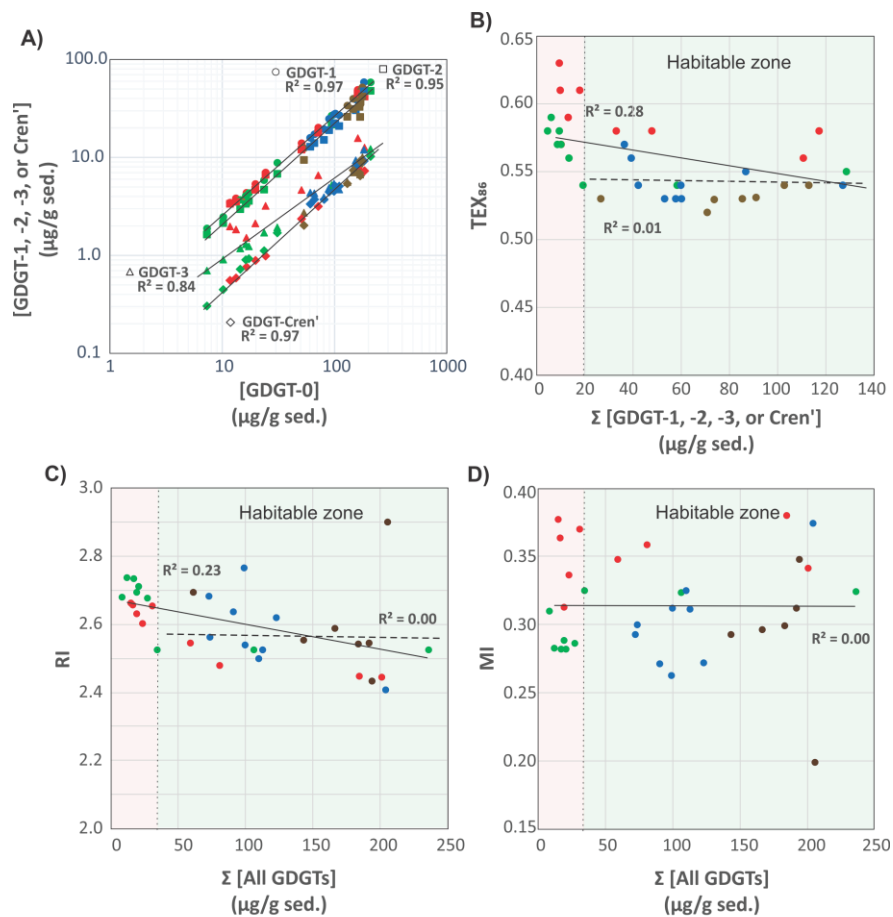


FIGURE 2. Down core profiles of the Cathedral Hill core *i*GDGTs absolute and relative lipid abundances and their generated *i*GDGT proxies: TEX₈₆, RI, and MI. Pink regions indicate transect intervals within zones of active GDGT lipid heterotrophy (Bentley et al., 2022). Grey regions mark regions where porewater temperatures exceed 123 °C marking a zone beyond the [known](#) upper thermal limit of life ([Kashefi and Lovley, 2003](#)). Yellow fields indicate regions where oil generation and hydrocarbon degradation ~~has~~ have been noted to occur (Dalzell et al., 2021).

Formatted: Font: 10 pt



• Core 1 • Core 2 • Core 3 • Core 4

FIGURE 3. A) Comparison of TEX₈₆ lipid concentrations GDGT-1 (circles), -2 (squares), -3 (triangles), and Cren' (diamonds) relative to the GDGT-0. Comparison of B) TEX₈₆, C) RI, and D) MI proxy values relative to summed iGDGTs abundances of the Cathedral Hill transect cores. Light green and pink regions indicate areas within and outside the habitable zone of life. Solid and dotted regression lines mark the total number of samples investigated for this study ($n=34$) and those that only reside within the habitable zone where up to 94% of the archaeal lipid turnover occurs ($n=22$), respectively.

3.2. TEX₈₆ and reconstructed SSTs

McClymont et al. (2012) reported a GDGT-based reconstructed annual SSTs of 16–18 °C ~~for from~~ particulate organic matter collected in ambient sediment traps in the Guaymas Basin during an annual cycle from 1996–1997. The reconstructed temperatures following the calibration model for sediments outside of polar regions proposed by Kim et al. (2010). These authors demonstrated the temperatures derived from the TEX₈₆ reconstruction were significantly lower than those produced by the closely co-varying U_{37}^{kv} , an alkenone lipid-based paleoclimate proxy (Brassell et al., 1986), and satellite measured estimates that jointly estimated a mean annual sea surface temperature (MASST) of 23 °C. The longer 21-year (1982–2004) satellite-derived MASST is also reported to be higher at 24 °C (Herrera-Cervantes et al., 2007). Although the sites and time frames of these surveys do not match that of the Cathedral Hill survey, they do provide context to what our reconstructed TEX₈₆ values should record.

The high sedimentation rate at Cathedral Hill has resulted in near homogenous inputs of organic matter from the upper water column across the transect area (Dalzell et al., 2021; Bentley et al., 2022). Therefore, TEX₈₆ reconstructions should produce equivalent cross-transect trends with sediment depth. Nonetheless, as with changes in the archaeal lipid concentrations, the profiles of iGDGT proxies TEX₈₆ and RI of the transect similarly have down core trends (Figure 2; Bentley et al., 2022). For core 4, TEX₈₆ span a narrow range of values ($n=7$; 0.52–0.54, avg. 0.53 ± 0.01 ; Figure 4A) across a period of ~ 37.5 to 75 yrs corresponding to the depth of the cores. To a slightly lesser degree, the shallow surface samples core top (0–2 cmbsf) across the transect also display near-equal values to core 4 ($n=4$; 0.56–0.54; avg. 0.55 ± 0.01). These values mark a TEX₈₆ reconstructed mean annual SST of 19.3–20.4 °C following the Kim et al. (2010) calibration model (Table 1). However, the TEX₈₆ values recorded in cores 1 to 3 at Cathedral Hill have considerably larger ranges with values spanning from 0.53 to 0.63 (Table 1) that systematically increase with rising porewater temperatures ($R^2 = 0.83$; Table 1; Figure 2 and 4A). This increase is most noticeable in core 1 where the highest TEX₈₆ values are obtained from the bottom core sediments (10–21 cmbsf; marking the non-habitable zone) where TEX₈₆ values span 0.57–0.63 (Table 1; Fig 4A) corresponding to a TEX₈₆ reconstructed SST change of 3.1 °C marking a range from 21.8 to 24.9 °C (Table 1). The Since the Cathedral Hill transect only spans ~8 m, the fundamental driver for the proxy's is likely influenced by the archaeal community composition that increases must be responding to their exposure to in situ vent fluid temperatures (Figure 4).

Two mechanisms are considered for the observed proxy variations. The first is that progressive ring-loss due to carbon-carbon bond cleavage of pentacyclic rings moieties by exposure to the sharp geothermal gradient acts to systematically attenuate the iGDGT lipid pool. Hydrous pyrolysis experiments conducted by Schouten et al. (2004) demonstrated that at extreme temperatures (ca. >160 °C), TEX₈₆ values become negatively impacted by the preferential destruction of polycyclic GDGTs. Such losses produce progressively lower ratio values. Although, the transect sediment porewaters do not reach the pyrolytic temperatures of the Schouten et al. (2004) experiment, they are high enough to generate hydrocarbons

Commented [JB44]: l. 408: if they were determined by vertical fluxes alone.

Commented [JB45]: l. 411: the “period of ~37.5 to 75 yrs” refers to which depth interval?

Commented [JB46]: l. 415: please specify “larger ranges”.

Commented [JB47]: l. 417: 10–21 cmbsf, i.e., the non-habitable zone mentioned above.

Formatted: Font: 10 pt

Formatted: Font: 10 pt

Commented [JB48]: l. 419–420: this could also be triggered by other processes than temperature that influence the archaeal community composition.

Commented [JB49R48]: Not wrong but how would you know

Formatted: Font: 10 pt

Formatted: Font: 12 pt

(Dalzell et al., 2021) and thermochemically degrade *i*GDGTs in the hottest regions of the transect [they are also more long-lived than what is produced from a laboratory experiment](#). However, the observed stratigraphic TEX₈₆ trends do not match those of predicted ring loss as the values increase rather than decrease in relation to elevated porewater condition. Nonetheless, the thermochemical oxidative loss of GDGTs and its effect on the TEX₈₆ ratio is further explored below (section 3.4).

The second mechanism is that subsurface microbial communities donate enough core GDGTs to overprint the detrital signal source. The RI (Figure 4B) values were similarly compared to recorded porewater temperatures to better interpret the TEX₈₆ trends and to ensure that the Cathedral Hill reconstructed temperatures are influenced by the subsurface microbial community. In this regard, RI is used to monitor the adaptive response of an archaeal community at the hydrothermal vent site. Lipid cyclization is an adaptive response to changing environmental temperature or acidity in which an archaeon increases its rigidity by decreasing the fluidity and permeability of its cellular membrane that, therefore, also further regulates the flow of solutes and nutrients in and out of the cell (Gliozzi et al., 1983; De Rosa and Gambacorta, 1988; Uda et al., 2001; Schouten et al., 2002; Macalady et al., 2004; Boyd et al., 2013). Both cores 1 and 2 have RI values highly correlated to temperature ($R^2 = 0.87$ and 0.75 , respectively) consistent with heat stress adaption. [This same was also observed in the Guaymas Basin by Schouten et al. \(2003\) who reported an increase in the RI of core lipid GDGTs with in situ temperature](#). As such, a significant proportion of the measured *i*GDGTs likely emanates from archaeal communities living in the shallow sediments of Cathedral Hill. As such, the lipid cyclization pattern may reflect stratigraphically discrete thermophilic to hyperthermophilic communities that are selectively adapted to more extreme temperature conditions (see Bentley et al., 2022 for further discussion on the lipid-based taxonomic make-up of the vent site).

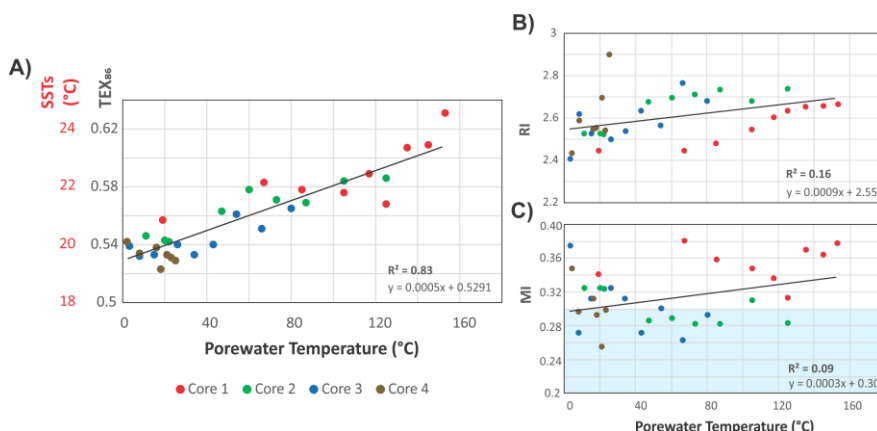


FIGURE 4. Cross plots of A) TEX₈₆, B) RI, and C) MI, *i*GDGT proxies versus porewater temperature. TEX₈₆^H reconstructed MASSTs are based on Kim et al. (2010). Blue field indicates MI values for normal marine conditions (Zang et al., 2011).

3.3. Lipid signal sourcing

To evaluate the sources of measured archaeal lipids, CL and IPL TEX₈₆ (the ratio applied to IPLs that contain equivalent core lipids) indices were compared as signal response loadings from their respective pools of living and dead cellular debris (Figure 5). For cores 1, 2, and 3 the 1G-*i*GDGT IPL TEX₈₆ measures are

Formatted: Left, Hyphenate

Commented [JB50]: Don't know if this belongs here

L. 479-489. Would be good to mention here that the same was observed in the Guaymas Basin by Schouten et al. (2003) who observed an increase in the RI of core lipid GDGTs with in situ temperature. Interestingly, they got a higher RI then observed here due mainly to a much lower relative abundances of crenarchaeol and a very high GDGT4. Can you speculate why your RI remains lower except for the deepest point in core 4?

Commented [JB51]: 1. 442-443: alternative ecological controls should be listed and discussed here (I assume data such as O2 or NH4 concentrations are not available to be compared to the TEX86 values?).

Commented [JB52R51]: correct

Formatted: Font: Font color: Auto

positively correlated with temperature ($R^2 = 0.46, 0.74$, and 0.66 , respectively; Figure 5A). In this regard, 1G-*i*GDGT IPL:TEX_{86} ratio appears to ~~also be largely measure-influenced by in situ~~ porewater temperatures as well as may by the archaeal community ecology of the vent system. Factors such as community composition and adaptation may further impact the IPL:TEX_{86} ratio as the rates of changes between cores 1–3 are not the same. Similar to the CL:TEX_{86} values, the IPL:TEX_{86} ~~are-is~~ not correlated to their summed TEX_{86} lipid abundances (Figure 5B). Such a condition is largely consistent with the living lipid pool being modified by the archaeal community's response to thermal stress and not by subsequent ~~thermal-oxidative~~ transformation occurring shortly after cell death.

The IPL and CL lipids of transect samples can be further grouped into three clusters (A, B, C), suggesting a mixed signal for the sourcing of archaeal GDGTs from both the living and dead pools of archaea (Figure 5C). In this plot, we assume that clusters falling on the 1:1 line indicate the living biota can equally contribute to the dead pool of total recovered GDGTs. Those off-axis contribute either less or more to one or the other lipid pool. The three clusters mark unique thermal zones within the transect area with cluster A being composed of the ambient core 2 to 4 seafloor surface samples; cluster B marking a mix of intermediate temperature samples from all cores; and cluster C being composed of high temperatures samples. The lipid groups likely mark distinct archaeal communities. As cluster B resides on the 1:1 line, the TEX_{86} core lipids likely have a ~~mixed-mix~~ of detrital and *in situ* inputs. Cluster C, however, appears likely dominated by *in situ* lipid production. The hyperthermophilic *Methanopyrus kandleri*, recovered from other Guaymas Basin sites (Teske et al., 2014), may represent one such archaeon contributing to the cluster C lipid pool. The thermal zonation and equivalent directionality of the resulting ratios (~~i.e.i.e.~~ both CL and IPL:TEX_{86} ratios increase with porewater temperature) further supports overprinting of the original CL:TEX_{86} sea surface signal by the ocean bottom sediment archaeal community as a mechanism for the observed CL:TEX_{86} trends.

Collectively, these results suggest the source of the archaeal core lipids measured in the TEX_{86} and RI indices progressively become more dominated by subsurface microbial communities adapted to the hotter hydrothermal vent fluids. Our results also indicate that in select natural environments, such as hydrothermal vent complexes, the TEX_{86} SST-proxy may ~~entirely record ocean bottom sediment porewater temperatures~~. To our knowledge, a clear case of overprinting to this level has not yet been demonstrated.

Commented [JB53]: 1. 461-480: I am missing a discussion about the other potential ecological controls on TEX_{86} values and, as is, the discussion only distinguishes 'living' and 'dead' archaea, but does not address the influence on TEX_{86} through changes in the contributions of Thaumarchaeota / Euryarchaeota (ANME?)/Bathyarchaeota etc. as well as potential ecotype contributions (even if the observed TEX_{86} trends are entirely determined by temperature, these archaea may not have the same response to adapt their membrane to temperature).

Commented [JB54]: 1. 479: if TEX_{86} "may entirely record ocean bottom sediment porewater temperatures", why are the calculated SSTs not maxed out in all samples (e.g., at $0.9=40^\circ\text{C}$)?

Commented [JB55R54]: I think that this is a very narrow view of thought. If the reviewer took the time to think about how the math works they would likely figure out that the relationship likely has an asymptote and it would never max out. Additionally, the cores are subject to various temperatures. Idk I see this as a pretty derpy comment

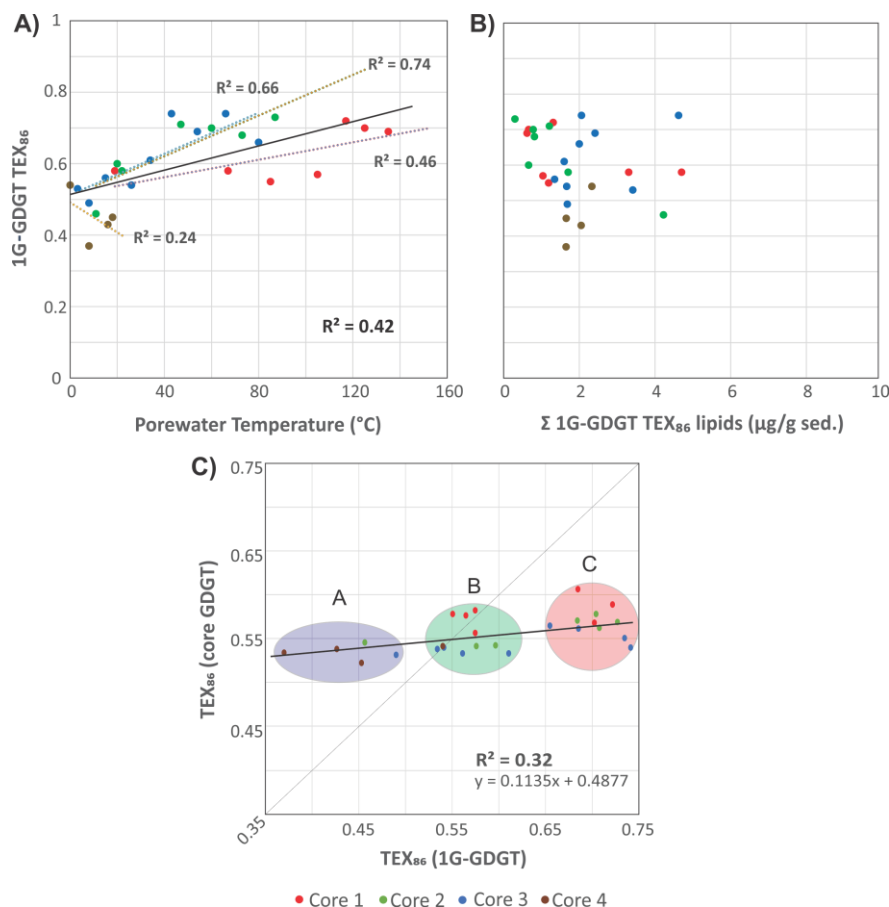


FIGURE 5. Cross plots of 1G-iGDGTs IPL TEX₈₆ versus (A) porewater temperatures and (B) the concentration of 1G-iGDGTs in the sediments. (C) TEX₈₆ proxy of core GDGTs vs 1G-GDGTs. Clusters A–C may represent different-different archeal communities that are providing varying inputs of iGDGT to the core GDGT lipid pool. The dotted trendline is the partial-partial least square regression of the complete core lipid TEX₈₆ data set. The solid line marks the 1:1 CL to IPL proxy correspondence-correspondence indicating both allochthonous and autochthonous sources contribute equally to the core GDGT lipid pool.

3.4. TEX₈₆ overprint corrections

The measured TEX₈₆ (M/TEX_{86}) value of the Cathedral Hill sediments is herein considered to be a weighted sum of a sea surface TEX₈₆ (ss/TEX_{86}) value acquired from lipids sourced in the upper water column that is further modified by a component of the deeper water column sourced core lipids (wc/TEX_{86}) as well as by additions of archaeal lipids from the benthic and subsurface microbial communities (sed/TEX_{86}). These ratio

Commented [JB56]: 1. 481: it would be very helpful if the symbols in Fig. 5C would allow the reader to differentiate the origin of the samples in the clusters. One would assume that cluster C is only made up of samples from the non-habitable zone, but this does not seem to be the case (includes 4 samples from core 3, which is 'habitable' in its entirety. Are there any trends, are these the lower samples or is there no pattern whatsoever?

Commented [JB57]: Not sure exactly where this one fits?

L.527-529. I apologize for repeating myself here, but was this not already shown in Schouten et al., 2003, i.e. a replacement of pelagic GDGTs with GDGTs of thermophilic archaea? Other studies which have documented overprints of pelagic GDGTs are those of sedimentary sulfate-methane transition zones where GDGTs of AOM archaea (GDGTs 1-3) overprint GDGTs and thereby impact TEX₈₆ values. This is one of the reasons why the MI index was developed by Zhang et al (2011) to check for this overprint. Would be good to mention this example here.

loadings are collectively also potentially further modified by diagenetic influences in the ocean bottom sediments. Over the cumulative sediment burial period and in consideration of the measured porewater temperatures of the Cathedral Hill push core sediments, these influences include the selective loss of lipids by their binding into protokerogen (K) and by potential changes due to the loss of lipid by turnover (ϕ ; section 3.1). Additional catagenetic effects from thermochemical alteration of lipids (θ) may also attenuate the sum of sedimentary core lipids by their exposure to high temperature vent fluids. Collectively, these effects are considered to form the following relationship:

$${}_M\text{TEX}_{86} = \frac{a_{SS}\text{TEX}_{86} + b_{WC}\text{TEX}_{86} + c(d_{0-n})_{Sed}\text{TEX}_{86}}{\phi + K + \theta} \quad (73)$$

where a , b , and c , are measured scaling parameters for lipid loading and ϕ , K , and θ are diagenetic and catagenetic alteration parameters. Solving for ${}_{SS}\text{TEX}_{86}$:

$${}_{SS}\text{TEX}_{86} = \frac{{}_M\text{TEX}_{86}(\phi + K + \theta)}{a} - \frac{b_{WC}\text{TEX}_{86} + c(d_{0-n})_{Sed}\text{TEX}_{86}}{a} \quad (84)$$

In this regard, a portion of the archaeal community from the deeper-upper water column, presumably initially sourced of IPLs, and an additional community inhabiting the ocean floor sediments ~~are-were~~ assumed to eventually die with their respective IPLs gradually becoming converted to CLs that further contribute to the observed ${}_M\text{TEX}_{86}$ value. For this study, no data ~~were-was~~ collected to calculate $b_{WC}\text{TEX}_{86}$ and its potential impact on ${}_M\text{TEX}_{86}$ ~~is-cannot be~~ further ~~consideredconsidered in this study~~. However, it is highly likely, given the longer residence times for glycosidic-based headgroups of the identified archaeal IPLs and their relatively short settling time through the water column (Lengger et al., 2012) that a component of this lipid source ~~could-was~~ already ~~be~~-mixed with the ${}_{Sed}\text{TEX}_{86}$ loading. For this study, ${}_{Sed}\text{TEX}_{86}$ is an ${}_{IPL}\text{TEX}_{86}$ ratio based on detected 1G-GDGT-1, -2, -3, and Cren' and 2G-GDGT-1, -2, as present in the original paleoclimate proxy (Eq. 4; Table 1; Figure 6). ~~The Testing the removal of 2G-GDGTs lipids, which have a low absolute concentration (<2 $\mu\text{g g}^{-1}$ sed.) and shallow stratigraphic zones of occurrence (section 3.1; Table S2), yielded 2G-GDGT a negligible <1 $^{\circ}\text{C}$ change in the summed average reconstructed SST lipids are excluded from the~~

~~calculation due to their low absolute concentrations (<2 $\mu\text{g g}^{-1}$ sed.), their limited number of detected TEX_{86} core lipid configurations (comprising only of GDGT 1 and GDGT 2; Table A2), and their short stratigraphic zones of occurrence (section 3.1). The $c(d_{0-n})_{Sed}\text{TEX}_{86}$ measured scaling parameter is further sealed by was calculated as~~

$$c(d_{0-n}) = \sum_{i=0}^n \left(\frac{[\text{GDGTs}]_{IPL-\text{TEX}_{86} \text{ lipids}}_n}{[\text{GDGTs}]_{CL-\text{TEX}_{86} \text{ lipids}}_{0-2cm}} \right) \quad 5)$$

~~the-using the summed concentrations of these lipids as they 1G- and 2G-GDGTs- that have the potential to become converted to GDGTs by progressive burial diagenesis increasingly- accumulate with sediment depth and (d_{0-n}) marking the range of sampled sediment depths, with 0 being the 0-2cmbsf core top and n the deepest point of sediment burial. These intervals are divided by the -The sum of allochthonous-water column input of TEX_{86} lipids ($\sum [\text{GDGTs}]_{CL-\text{TEX}_{86} \text{ lipids}}_{0-2cm}$) is estimated to be 120 $\mu\text{g g}^{-1}$ sed. based on an average measured surface lipid concentration (0-2cmbsf)-measured across the four-core transect. As such,~~

$$c(d_{0-n}) = \sum_{i=0}^n \left(\frac{[\text{GDGTs}]_{IPL-\text{TEX}_{86} \text{ lipids}}_n}{[\text{GDGTs}]_{CL-\text{TEX}_{86} \text{ lipids}}_{0-2cm}} \right) \quad (9)$$

~~where n is the deepest point of sediment bThe function ural (further-assumes the that the surface sediment layer 0-2cmbsf does not having have any component of hydrolyze its its IPL- GDGTs converted to CLs (-Table 2). When applied to Eq. 4 and further excluding ϕ , K , and θ , the ${}_{SS+WC}\text{TEX}_{86}^H$ reconstructed~~

Formatted: Font: Italic, Subscript

Commented [JB58]: 1. 514: in line 314, the number is ~7 $\mu\text{g/g}$ DW

Commented [JB59]: 1. 514-515: I understand the mass balance argument, but the fact that 2G-GDGTs only come with 1 or 2 cyclopentyl moieties could actually bias TEX_{86} much more profoundly (thus, is not a good argument).

Commented [JB60R59]: Again, how would it be a bad argument when it would be a minor component of the equation, not impacting it?

Formatted: Font: Italic

Formatted: Indent: Left: 3.81 cm, First line: 1.27 cm

Formatted: Font: Italic

Formatted: Superscript

Commented [JB61]: 1. 517-524: I am getting lost here, there is too much information missing. What is the definition of "allochthonous"? Why sum the GDGT concentrations for the entire depth interval (as implied by the upper bound n) if the goal is to correct the TEX_{86} values in a distinct depth interval? Shouldn't the correction only scale the abundance of GDGTs in that particular interval against the original input rather than summing the concentration in the total sediment column? Why would the core-top not already have lost some of the IPLs? Sedimentation rates of 0.4–0.2 cm/yr imply that a 0-2cm core-top integrates 5-10 years of deposition.

Formatted: Justified

Formatted: Justified, Indent: Left: 0 cm, First line: 0 cm

SSTs average temperature of 19.68 ± 0.79 °C (Table 2; Figure 6A) mirroring the range of values measured in the ambient sediments of core 4.

The selective lipid removal by diagenetic and catagenetic processes theoretically may also affect the TEX₈₆ value; however, their perspective impact on the directionality and magnitude of the ratio are difficult to predict and equally hard to discretely measure. For Cathedral Hill, although the loss of GDGTs to protokerogen formation could potentially impact the ratio, it has been proven shown to be a very low negligible sink for the lipids analyzed sediments (Bentley et al., 2022). As such, the selectivity of lipid classes being adsorbed to a protokerogen is undeterminable. More importantly, for this site it is insignificant, and the K parameter in Eqs. 7-3 and 8-4 is therefore assigned a θ value of 0.

The degradation rates of each TEX₈₆ lipid class were independently measured for the four push cores (Eq. 6; Fig. A2). Given Due to the high geothermal gradient at Cathedral Hill, some of the transect push core sediments resided within zones of active catagenesis (Fig. 2; Dalzell et al., 2021). The degradation rates of each TEX₈₆ lipid was independently measured for the four push cores (Eq. 2; Fig. S2). As the abundance of both CLs and IPLs differentially decreases through the various core sediment profiles with turnover rates that appear to be constrained by porewater temperature changes (section 3.1), the degradation rates must also record the effects of thermochemical oxidative weathering (Fig. 3B). In this case, ϕ and θ are therefore treated as a grouped parameter parameters.

To determine if individual lipid classes were selectively removed during degradation, the variance (s^2) of the rate change as measured from its respective regression slope (i.e. $m_{\log k}$) of from the TEX₈₆ lipids classes (Fig. A2S2; Supplemental-Table A3-S4 from Eq. 62) were calculated. For the Cathedral Hill transect, the calculated $m_{\log k}$ s^2 is 0.4420, which suggests near equal degradation rates for all TEX₈₆ lipid classes. Therefore, lipid turnover and the concomitant thermochemical oxidation of these lipid classes is also similarly largely non-selective. A weighing function for the degree of lipid class selectivity during turnover is nonetheless proposed:

$$\phi + \theta = 1/M \text{TEX}_{86}^{0.442} \quad (406)$$

When applied to Eq. 8-4, is obtained. The corrected data series produces an average transect $_{SS+W} \text{TEX}_{86}^H$ reconstructed SST of 23.66 ± 0.59 °C with a near-zero partial least squares regression slope (Table 2; Figure 6B). The marginal change is likely due to samples from cores 1 and 2 that display evidence of *in situ* hydrocarbon generation associated with thermochemical oxidation (Dalzell et al., 2021). As these modeled values are within the 23–24 °C obtained for the 21-year (1982–2004) satellite-derived MASST data for the Guaymas Basin region (Herrera-Cervantes et al., 2007). Based on these calculations, nearly all $M \text{TEX}_{86}$ attenuation can be attributed to sediment microbial overprinting consistent with prior observations at Guaymas Basin (Schouten et al., 2003; Zhang et al., 2011), lipid by turnover and thermochemical alteration of lipids. The high degree of influence is striking given that the upper water flux of GDGTs at Cathedral Hill is estimated to represents up to 93% of the total intact polar and core GDGT lipid pool within these sediments. In this regard, this study demonstrates the benthic microbial community can influence TEX₈₆ measurements. minor changes to the reconstructed lumped $_{SS+W} \text{TEX}_{86}$ ratio are observed consistent with the absence of a comparative relationship between i GDGT down core lipid depletions and the respective $M \text{TEX}_{86}$ ratios across the biologically active zone of the transect sediments (section 3.1; Figure 3B).

The high degree of influence is striking given that the upper water flux of GDGTs is estimated to represents up to 93% of the total intact polar and core GDGT lipid pool within these sediments.

Equation 7 predicts an average transect $_{SS+W} \text{TEX}_{86}^H$ reconstructed SST of 21.92 ± 0.66 °C with no elevated trends for increasing porewater temperatures across each of the transect cores (Table 2; Figure 6A). The

Commented [JB62]: 1. 526-532: this section is at odds with the discussion regarding the kinetic model and the last two sentences directly contradict each other "...the selectivity of lipid classes being adsorbed to a protokerogen is undeterminable. More importantly, for this site it is insignificant...".

Commented [JB63]: 1. 536-538: there is no discussion on IPL turnover rates in section 3.1 and only a sentence linking GDGT turnover rates to hydrothermalism (citing the findings of Bentley et al. 2022). How GDGT and IPL concentrations compare downcore would be a useful addition to Fig. 2 or at least it could be expressed here using statistical means (Kruskal-Wallis).

Commented [JB64]: 1. 566: how is a "high degree of influence" assessed? It will be worthwhile to compare the offset in light of the calibration residuals.

Formatted: Font color: Auto

Commented [JB65]: 1. 566: how is a "high degree of influence" assessed? It will be worthwhile to compare the offset in light of the calibration residuals.

corrected data series show a lack of correlation associated with a near-zero PLS regression slope, suggesting the model backs out the original SST signal. If the ϕ , K , and θ scaling parameters are removed from the calculation the average temperature shifts 2.08°C lower to $19.69 \pm 0.39^\circ\text{C}$ (Table 2; Figure 6B). The marginal change is likely due to only a few sediment samples displaying evidence of *in situ* hydrocarbon generation associated with thermochemical oxidation (Dalzell et al., 2021). Irrespective of the approach, but particularly the case for the more simplified expression, all measures produce values closer to the expected SST of $19.3\text{--}20.4^\circ\text{C}$ that is based on the range of values recorded for core 4 and the three transect surface sediments (section 3.2). These values are $\sim 3^\circ\text{C}$ lower than the $23\text{--}24^\circ\text{C}$ obtained for the 21 year (1982–2004) satellite-derived MASST data for the Guaymas Basin region (Herrera-Cervantes et al., 2007). Nonetheless, nearly all $m\text{TEX}_{86}$ attenuation can therefore be attributed to sediment microbial overprinting. The high degree of influence is striking given that the upper water flux of GDGTs is estimated to represent up to 93% of the total intact polar and core GDGT lipid pool within these sediments. In this regard, it demonstrated that microbial community influences TEX_{86} measurements.

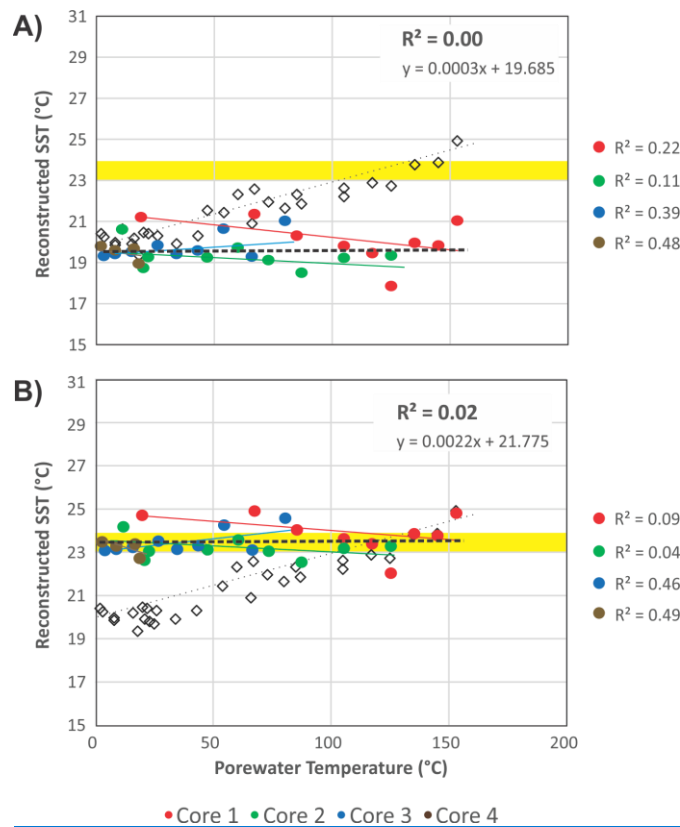


FIGURE 6. Reconstructed combined $s\text{TEX}_{86}$ and SSTs $w\text{TEX}_{86}$ from Eq. 4 (A) Eq. 8 with and (B) Eq. 8 without ϕ , K , and θ scaling parameters compared to measured porewater temperatures. Red, green, blue,

Commented [JB66]: 1. 564-565: what is the explanation for this 3°C offset relative to the actual SST? This seems to be an important discussion to be had given that the suggested TEX_{86} -correction effectively accounts for a similar offset (some $3\text{--}4^\circ\text{C}$).

Commented [JB67]: 1. 566: how is a “high degree of influence” assessed? It will be worthwhile to compare the offset in light of the calibration residuals.

Formatted: Centered

Formatted: Font: Not Bold

Formatted: Font: Not Bold

710 and brown circles indicate recorded values from cores 1, 2, 3, and 4, respectively. $MTEX_{86}$ values are plotted
711 for reference (open black diamonds). Yellow field is the 23–24 °C range observed for the 21-year (1982–
712 2004) satellite-derived MASST data (Herrera-Cervantes et al., 2007).
713
714
715

716
717

Table 2. Reconstructed sea surface temperatures.

Sample	Depth (cmbsf)	Porewater Temp. (°C)	<i>t</i> Time (yrs.)	$\delta^{18}\text{O}_{\text{TEX}_{86}}$ (Measured iGDGT TEX ₈₆)	Reconstructed SST (°C)	TEX ₈₆ 1G- & 2G- GDGT IPLs ($\mu\text{g g}^{-1}$)	Cumulative 1G- & 2G- GDGTs Loading with Depth ($\mu\text{g g}^{-1}$)	$\delta^{18}\text{O}_{\text{TEX}_{86}}$ (i.e. 1G- & 2G-GDGT w/TEX ₈₆)	$c(\text{do})$ Cumulative Weighted Loading (%)
Core 1 (0-2cm)	1	19	10	0.56	21.2	4.80	0	0.580-58	0.00
Core 1 (2-4cm)	3	67	20	0.58	22.6	3.41	4.80	0.580-58	0.04
Core 1 (4-6cm)	5	85	30	0.58	22.3	1.29	8.21	0.550-55	0.07
Core 1 (6-8cm)	7	105	40	0.58	22.2	1.14	9.50	0.570-57	0.08
Core 1 (8-10cm)	9	117	50	0.59	22.9	1.41	10.64	0.720-72	0.09
Core 1 (10-12cm)	11	125	60	0.57	21.8	0.76	12.05	0.700-70	0.10
Core 1 (12-15cm)	13	135	70	0.61	23.8	0.72	12.81	0.690-69	0.11
Core 1 (15-18cm)	17	145	80	0.61	23.9	0.00	13.53	0.690-69	0.11
Core 1 (18-21cm)	20	153	90	0.63	24.9	0.00	13.53	0.690-69	0.11
Avg.				0.59	22.84				
Std. Dev.				0.02	1.16				
Core 2 (0-2cm)	1	11	10	0.55	20.6	4.33	0	0.490-46	0.00
Core 2 (2-4cm)	3	22	20	0.54	20.4	1.80	4.33	0.570-58	0.04
Core 2 (4-6cm)	5	20	30	0.54	20.5	0.76	6.13	0.600-60	0.05
Core 2 (6-8cm)	7	47	40	0.56	21.5	1.31	6.89	0.730-71	0.06
Core 2 (8-10cm)	9	60	50	0.58	22.3	0.88	8.20	0.700-70	0.07
Core 2 (10-12cm)	11	73	60	0.57	22.0	0.92	9.08	0.680-68	0.08
Core 2 (12-15cm)	13	87	70	0.57	21.8	0.40	10.00	0.730-73	0.08
Core 2 (15-18cm)	17	105	80	0.58	22.6	0.00	10.40	0.730-73	0.09
Core 2 (18-21cm)	20	125	90	0.59	22.7	0.00	10.40	0.730-73	0.09
Avg.				0.56	21.61				
Std. Dev.				0.02	0.91				
Core 3 (0-2cm)	1	3.2	10	0.54	20.2	3.51	0	0.560-53	0.03
Core 3 (2-4cm)	3	8	20	0.53	19.9	1.79	3.51	0.510-49	0.01
Core 3 (4-6cm)	5	15	30	0.53	19.9	1.45	5.30	0.570-56	0.01
Core 3 (6-8cm)	7	26	40	0.54	20.3	1.77	6.74	0.550-54	0.01
Core 3 (8-10cm)	9	34	50	0.53	19.9	1.70	8.51	0.610-61	0.01
Core 3 (10-12cm)	11	43	60	0.54	20.3	2.16	10.21	0.710-74	0.02
Core 3 (12-15cm)	13	54	70	0.56	21.4	2.52	12.37	0.690-69	0.02
Core 3 (15-18cm)	17	66	80	0.55	20.9	4.72	14.89	0.730-74	0.04
Core3 (18-21cm)	20	80	90	0.57	21.6	2.10	19.61	0.650-66	0.02
Avg.				0.54	20.50				
Std. Dev.				0.01	0.67				
Core 4 (0-2cm)	1	2	10	0.54	20.4	2.43	0	0.540-54	0.02
Core 4 (2-4cm)	3	8	20	0.53	20.0	1.75	2.43	0.440-37	0.01
Core 4 (4-6cm)	5	16	30	0.54	20.2	2.15	4.18	0.490-43	0.02

Core 4 (6-8cm)	7	18	40	0.52	19.3	1.76	6.34	0.470.45	0.01
Core 4 (8-10cm)	9	21	50	0.53	19.9	0.44	8.09	-	-
Core 4 (10-12cm)	11	23	60	0.53	19.8	2.20	8.54	-	-
Core 4 (12-15cm)	13	25	70	0.53	19.7	0.00	10.74	-	-
Avg.				0.53	19.90				
Std. Dev.				0.01	0.34				
Cumulative Avg.					19.68				
Cumulative Std. Dev.					0.79				

* Marks inherited values from the above sediment horizon.

- Formatted: Font: 8 pt
- Formatted: Font: 8 pt
- Formatted: Font: 8 pt
- Formatted Table
- Formatted: Font: 8 pt
- Formatted: Font: 8 pt
- Formatted Table
- Formatted: Font: 8 pt
- Formatted: Font: 8 pt
- Formatted: Font: Bold
- Formatted: Font: 8 pt, Bold
- Formatted: Font: 8 pt
- Formatted: Font: 8 pt, Bold
- Formatted: Font: 8 pt, Bold
- Formatted: Font: 8 pt
- Formatted: Font: 12 pt

Table 2. Reconstructed sea surface temperatures (continued).

Sample	Eq. 8.4 excluding $\phi+\theta+K$			Eq. 8.4 including $\phi+\theta+K$		
	$SS+WC\overline{TEX}_{86}$ ($n\overline{TEX}_{86} - c(d\phi_n)^*_{Std}\overline{TEX}_{86}$)	$SS+WC\overline{TEX}_{86}^H$ (after Kim et al., 2010)	$SS+WC\overline{TEX}_{86}^H$ Reconstructed SST ($^{\circ}C$)	$\phi+\theta$ (Eq. 4.6) (where $s^2 = 0.11$; Table A3S3)	$SS+WC\overline{TEX}_{86}$	$SS+WC\overline{TEX}_{86}^H$ Reconstructed SST ($^{\circ}C$) (after Kim et al., 2010)
Core 1 (0-2cm)	0.56	-0.25	21.2	1.124.07	0.630.59	24.723.1
Core 1 (2-4cm)	0.56	-0.25	21.4	1.124.07	0.630.60	24.923.3
Core 1 (4-6cm)	0.54	-0.27	20.3	1.134.07	0.620.58	24.222.5
Core 1 (6-8cm)	0.53	-0.27	19.8	1.134.07	0.610.57	23.922.0
Core 1 (8-10cm)	0.52	-0.28	19.5	1.144.07	0.610.57	23.724.8
Core 1 (10-12cm)	0.50	-0.30	17.9	1.154.08	0.580.54	22.620.5
Core 1 (12-15cm)	0.53	-0.27	20.0	1.134.07	0.620.58	24.222.3
Core 1 (15-18cm)	0.53	-0.27	19.8	1.134.07	0.610.58	24.122.2
Core 1 (18-21cm)	0.55	-0.26	21.0	1.134.07	0.630.60	25.023.2
Avg.	0.54	-0.27	20.10	1.134.07	0.610.58	24.1422.33
Std. Dev.	0.02	0.02	1.08	0.010.00	0.020.02	0.750.89
Core 2 (0-2cm)	0.55	-0.26	20.6	1.134.07	0.620.58	24.222.6
Core 2 (2-4cm)	0.52	-0.28	19.2	1.144.07	0.600.56	23.324.5
Core 2 (4-6cm)	0.51	-0.29	18.7	1.144.08	0.590.55	22.924.1
Core 2 (6-8cm)	0.52	-0.28	19.3	1.144.07	0.600.56	23.424.6
Core 2 (8-10cm)	0.53	-0.28	19.7	1.144.07	0.610.57	23.822.0
Core 2 (10-12cm)	0.52	-0.28	19.1	1.144.07	0.600.56	23.424.5
Core 2 (12-15cm)	0.51	-0.29	18.5	1.144.08	0.590.55	23.024.0
Core 2 (15-18cm)	0.52	-0.28	19.2	1.144.07	0.600.56	23.524.6
Core 2 (18-21cm)	0.52	-0.28	19.3	1.144.07	0.600.57	23.624.7
Avg.	0.52	-0.28	19.32	1.144.07	0.600.56	23.4721.64
Std. Dev.	0.01	0.01	0.60	0.000.00	0.010.01	0.400.49
Core 3 (0-2cm)	0.52	-0.28	19.4	1.144.07	0.600.56	23.324.5
Core 3 (2-4cm)	0.52	-0.28	19.4	1.144.07	0.600.56	23.324.6
Core 3 (4-6cm)	0.53	-0.28	19.5	1.144.07	0.600.57	23.424.7
Core 3 (6-8cm)	0.53	-0.27	19.9	1.134.07	0.600.57	23.624.9
Core 3 (8-10cm)	0.52	-0.28	19.4	1.144.07	0.600.56	23.324.6
Core 3 (10-12cm)	0.53	-0.28	19.6	1.144.07	0.600.57	23.524.7
Core 3 (12-15cm)	0.55	-0.26	20.7	1.134.07	0.620.59	24.322.7
Core 3 (15-18cm)	0.52	-0.28	19.3	1.144.07	0.600.56	23.424.5
Core 3 (18-21cm)	0.55	-0.26	21.0	1.134.07	0.620.59	24.623.0
Avg.	0.53	-0.27	19.79	1.144.07	0.600.57	23.6421.94
Std. Dev.	0.01	0.01	0.62	0.000.00	0.010.01	0.490.55
Core 4 (0-2cm)	0.53	-0.27	19.8	1.134.07	0.600.57	23.624.9
Core 4 (2-4cm)	0.53	-0.28	19.7	1.144.07	0.600.57	23.424.8

Core 4 (4-6cm)	0.53	-0.28	19.8	1.144.07	0.600.57	23.524.9
Core 4 (6-8cm)	0.52	-0.29	19.0	1.144.08	0.590.56	22.924.2
Core 4 (8-10cm)	-	-	-	-	-	-
Core 4 (10-12cm)	-	-	-	-	-	-
Core 4 (12-15cm)	-	-	-	-	-	-
Avg.	0.53	-0.28	19.55	1.07	0.600.65	23.3821.67
Std. Dev.	0.01	0.01	0.39	0.00	0.010.01	0.310.35
Cumulative Avg.						23.66
Cumulative Std. Dev.						0.59
			19.71			21.92
			0.79			0.66

4. Conclusions

In this study, we demonstrate a pronounce overprint of ϵ GDGTs sourced from the ocean floor sedimentary archaeal community at the Cathedral Hill vent site in Guaymas Basin. The overprint is marked by lipids with more cyclized ring moieties marking an adaptive response by archaea to rigidify the cellular membranes against localized heat stress. For This in turn has this study, we demonstrate the resulted in the commonly used TEX₈₆ paleoclimate proxy to can become heavily impacted by the ocean floor archaeal community. For the Cathedral Hill vent site at Guaymas Basin, the lipids sourced from these sediments resulted in TEX₈₆ reconstructed temperatures that partially record conditions of the advecting porewaters temperatures. However, As the vast majority of ϵ GDGTs in these sediments is sourced from the overlying water column, the impact on the TEX₈₆ ratio is further the product of he impact appears to result from a combination of source inputs rapid lipid turnover rates and ,their diagenetic and catagenetic alteration; processes potentially unique to the hydrothermal system, and further overprint by the additions of lipids from the ocean floor sedimentary archaeal community that has adapted to the high temperature conditions of the vent fluids by producing more cyclized ring moieties to rigidify their cellular membranes. Together, these processes factors resulted in absolute TEX₈₆^H temperature offsets of up to 4 °C based on calibrations closely suited to the latitudinal position of Guaymas Basin. Such large offsets could be meaningful to paleoclimate reconstructions (i.e. global changes by 2-4 °C mean completed deglaciation). As such, To untangle the impact of these coupled drivers on the TEX₈₆ proxy, we further further present a method to correct the overprints by both the water column and subsurface archaeal community's community using IPLs extracted from both of these sources. Although, we have not been able to test this model with lipid inputs from the overlying water column, we have demonstrated its effectiveness at removing sediment sourced overprints, which may not be unique to hydrothermal systems. This approach should be capable of being extended to all near-surface marine sediment systems and may improve the quality of calibration models or climate reconstructions that are based on-on modern TEX₈₆ measures.

Conflicts of Interest

The authors declare no conflict of interest.

Supplementary information

Supplementary material related to this article can be found on-line at <https://doi.org/.....>

Formatted: Font: 8 pt

Formatted: Font: 8 pt

Formatted: Font: 8 pt

Formatted: Font: 8 pt

Formatted: Font: 8 pt

Formatted: Font: 8 pt

Formatted: Font: 8 pt

Formatted: Font: 8 pt

Formatted: Font: 8 pt

Formatted: Font: 8 pt

Formatted: Font: 8 pt

Formatted: Font: 8 pt

Formatted: Font: 8 pt

Formatted: Font: 8 pt

Formatted: Font: 8 pt

Formatted: Font: 8 pt

Formatted: Font: 8 pt

Formatted: Font: 8 pt

Formatted: Font: 8 pt

Formatted: Font: 8 pt

Formatted: Font: 8 pt

Formatted: Font: 8 pt

Formatted: Font: 8 pt

Formatted: Font: 8 pt

Formatted: Font: 8 pt

Formatted: Font: 8 pt

Formatted: Font: 8 pt

Formatted: Font: 8 pt

Formatted: Font: 8 pt

Formatted: Font: 8 pt

Formatted: Font: 8 pt

Formatted: Font: 8 pt

Formatted: Font: 8 pt

Formatted: Font: 8 pt

Formatted: Font: 8 pt

Formatted: Font: 8 pt

Formatted: Font: 8 pt

Formatted: Font: 8 pt

Formatted: Font: 8 pt

Formatted: Font: 8 pt

Formatted: Font: 8 pt

Formatted: Font: 8 pt

Formatted: Font: 8 pt

Formatted: Font: 8 pt

Formatted: Font: 8 pt

Formatted: Font: 8 pt

Formatted: Font: 8 pt

Formatted: Font: 8 pt

Formatted: Font: 8 pt

Commented [JB68]: 1. 597-598: what is the meaning of "global changes by 2-4°C mean completed deglaciation" and, more importantly, which reference does this statement refer to?

Commented [JB69R68]: Isn't this a bit of a stretch? It isn't a global average it's a local average is it not?

Formatted: Subscript

References

- Bentley, J. N., Ventura, G. T., Dalzell, C. J., Walters, C. C., Peters, C. A., Mennito, A. S., Nelson, R. K., Reddy, C. M., Walters, C. J., Seewald, J., & Sievert, S. M. (2022). Archaeal lipid diversity, alteration, preservation at Cathedral Hill, Guaymas Basin, and its link to the deep time preservation paradox. *Organic Geochemistry*, 163:104302. doi.org/10.1016/j.orggeochem.2021.104302.
- Besseling, M., Hopmans, E. C., Koenen, M., van der Meer, M. T. J., Vreugdenhil, S., Schouten, S., Sinninghe Damsté, J. S., & Villanueva, L. (2019). Depth-related differences in archaeal populations impact the isoprenoid tetraether lipid composition of the Mediterranean Sea water column. *Organic Geochemistry*, 135, 16–31. doi.org/10.1016/j.orggeochem.2019.06.008.
- Besseling, M. A., Hopmans, E. C., Bale, N. J., Schouten, S., Sinninghe Damsté, J. S., & Villanueva, L. (2020). The absence of intact polar lipid-derived GDGTs in marine waters dominated by Marine Group II: Implications for lipid biosynthesis in Archaea. *Sci Rep* 10, 294. doi.org/10.1038/s41598-019-57035-0.
- Biddle, J. F., Cardman, Z., Mendlovitz, H., Albert, D. B., Lloyd, K. G., Boetius, A., & Teske, A. (2012). Anaerobic oxidation of methane at different temperature regimes in Guaymas Basin hydrothermal sediments. *The ISME Journal* 6, 1018–1031. doi.org/10.1038/ismej.2011.164.
- Boetius, A., Ravensschlag, K., Schubert, C., Rickert, D., Widdel, F., Gieseke, A., Amann, R., Jørgensen, B.B., Witte, U., & Pfannkuche, O. (2000). A marine microbial consortium apparently mediating anaerobic oxidation of methane. *Nature* 407, 623–626. https://doi.org/10.1038/35036572.
- Boyd, E., Hamilton, T., Wang, J., He, L., & Zhang, C. (2013). The role of tetraether lipid composition in the adaptation of thermophilic archaea to acidity. *Frontiers in Microbiology*, 4, 62.
- Brochier- Armanet, C., Boussau, B., Gribaldo, S., & Forterre, P. (2008). Mesophilic Crenarchaeota: proposal for a third archaeal phylum, the Thaumarchaeota. *National Review Microbiology* 6, 245–252. doi:10.1038/nrmicro1852.
- Carr, S. A., Schubotz, F., Dunbar, R. B., Mills, C. T., Dias, R., Summons, R. E., & Mandernack, K. W. (2018). Acetoclastic Methanosaeta are dominant methanogens in organic-rich Antarctic marine sediments. *The ISME Journal*, 12(2), 330–342. https://doi.org/10.1038/ismej.2017.150.
- Curry, J. R., Moore, D. G., Lawver, L. A., Emmel, F. J., Raitt, R. W., Henry, M., & Kieckhefer, R. (1979). Tectonics of the Andaman Sea and Burma: convergent margins. In J.S. Watkins, L. Montadert, P.W. Dickerson (Eds.) *Geological and Geophysical Investigations of Continental Margins*, AAPG Memoir 29, 189–198.
- Dalzell, C. J., Ventura, G. T., Nelson, R. K., Reddy, C. M., Walters, C. J., Seewald, J., & Sievert, S. M. (2021). Resolution of multi-molecular hydrocarbon transformation in petroleum-bearing sediments from the Cathedral Hill hydrothermal vent complex at Guaymas Basin, Gulf of California by comprehensive two-dimensional gas chromatography and chemometric analyses. *Organic Geochemistry*, 152, 104173.
- De Rosa, M., & Gambacorta, A. (1988). The lipids of archaeobacteria. *Progress in lipid research*, 27, 153–175.
- Elling, F.J., Könneke, M., Lipp, J.S., Becker, K.W., Gagen, E.J., & Hinrichs, K.-U. (2014). Effects of growth phase on the membrane lipid composition of the thaumarchaeon *Nitrosopumilus maritimus* and their implications for archaeal lipid distributions in the marine environment. *Geochimica et Cosmochimica Acta*, 141, 579–597.

- Elling, F. J., Könneke, M., Mußmann, M., Greve, A., & Hinrichs, K. U. (2015). Influence of temperature, pH, and salinity on membrane lipid composition and TEX₈₆ of marine planktonic thaumarchaeal isolates. *Geochimica et Cosmochimica Acta*, 171, 238–255.
- Gieskes, J. M., Simoneit, B. R., Brown, T., Shaw, T. J., Wang, Y. C., & Magenheimer, A. (1988). Hydrothermal fluids and petroleum in surface sediments of Guaymas Basin, Gulf of California: a case study. *The Canadian Mineralogist*, 26, 589–602.
- Gliozzi, A., Paoli, G., De Rosa, M., & Gambacorta, A. (1983). Effect of isoprenoid cyclization on the transition temperature of lipids in thermophilic archaeobacteria. *Biochimica et Biophysica Acta (BBA)-Biomembranes*, 735, 234–242.
- Herrera-Cervantes, H., Lluch-Cota, D. B., Lluch-Cota, S. E., & Gutiérrez-de-Velasco, S. G. (2007). The ENSO signature in sea-surface temperature in the Gulf of California. *Journal of Marine Research*, 65, 589–605. doi.org/10.1357/002224007783649529.
- Herfort, L., Schouten, S., Boon, J. P. & Sinninghe Damsté, J. S. (2006). Application of the TEX₈₆ temperature proxy to the southern North Sea. *Organic Geochemistry* 37, 1715–26.
- Ho, S. L. & Laepple, T. (2016). Flat meridional temperature gradient in the early Eocene in the subsurface rather than surface ocean. *Nature Geoscience*, 9, 606–610.
- Hollis, C.J., Taylor, K.W.R., Handley, L., Pancost, R.D., Huber, M., Creech, J.B., Hines, B.R., Crouch, E.M., Morgans, H.E.G., Crampton, J.S., Gibbs, S., Pearson, P.N., & Zachos, J.C. (2012). Early Paleogene temperature history of the Southwest Pacific Ocean: Reconciling proxies and models. *Earth and Planetary Science Letters* 349–350, 53–66
- Hopmans, E. C., Weijers, J. W., Schefuß, E., Herfort, L., Sinninghe Damsté, J. S., & Schouten, S. (2004). A novel proxy for terrestrial organic matter in sediments based on branched and isoprenoid tetraether lipids. *Earth and Planetary Science Letters*, 224, 107–116.
- Huguet, C., Cartes, J. E., Sinninghe Damsté, J. S., & Schouten, S. (2006). Marine crenarchaeotal membrane lipids in decapods: Implications for the TEX₈₆ paleothermometer. *Geochemistry, Geophysics, Geosystems*, 7. doi 10.1029/2006GC001305.
- Huguet, C., Martrat, B., Grimalt, J. O., Sinninghe Damsté, J. S. & Schouten, S. (2011). Coherent millennial-scale patterns in U37 k0 and TEX₈₆ H temperature records during the penultimate interglacial-to-glacial cycle in the western Mediterranean. *Paleoceanography* 26. DOI: 10.1029/2010PA002048.
- Huguet, C., Schimmelmann, A., Thunell, R., Lourens, L. J., Sinninghe Damsté, J. S., & Schouten, S. (2007). A study of the TEX₈₆ paleothermometer in the water column and sediments of the Santa Barbara Basin, California. *Paleoceanography*, 22. doi 10.1029/2006PA001310.
- Hurley, S.J., Elling, F.J., Könneke, M., Buchwald, C., Wankel, S.D., Santoro, A.E., Lipp, J.S., Hinrichs, K.-U., Pearson, A. (2016). Influence of ammonia oxidation rate on thaumarchaeal lipid composition and the TEX₈₆ temperature proxy. *Proceedings of the National Academy of Sciences, U. S. A.* 113, 7762–7767.
- Kallmeyer, J., & Boetius, A. (2004). Effects of temperature and pressure on sulfate reduction and anaerobic oxidation of methane in hydrothermal sediments of Guaymas Basin. *Applied and Environmental Microbiology*. 70, 1231–1233. doi.org/10.1128/AEM.70.2.1231-1233.2004.
- Karner, M. B., DeLong, E. F., Karl, D. M. (2001). Archaeal dominance in the mesopelagic zone of the Pacific Ocean. *Nature*. 25, 409(6819), 507–510. doi: 10.1038/35054051.
- Kashefi, K., & Lovley, D. R. (2003). Extending the upper temperature limit for life. *Science*, 301, 934–934.

- Kim, J. H., Schouten, S., Hopmans, E. C., Donner, B., & Damsté, J. S. S. (2008). Global sediment core-top calibration of the TEX₈₆ paleothermometer in the ocean. *Geochimica et Cosmochimica Acta*, 72, 1154–1173.
- Kim, J. H., Van der Meer, J., Schouten, S., Helmke, P., Willmott, V., Sangiorgi, F., Koç, N., Hopmans, E. C. & Damsté, J. S. S. (2010). New indices and calibrations derived from the distribution of crenarchaeal isoprenoid tetraether lipids: Implications for past sea surface temperature reconstructions. *Geochimica et Cosmochimica Acta*, 74, 4639–4654.
- Kim J.-H., Romero O. E., Lohmann G., Donner B., Laepple T., Haam E. & Sinninghe Damsté J. S. (2012a) Pronounced subsurface cooling of North Atlantic waters off Northwest Africa during Dansgaard-Oeschger interstadials. *Earth and Planetary Science Letters*, 339–340, 95–102.
- Kim, J. H., Crosta, X., Willmott, V., Renssen, H., Bonnin, J., Helmke, P., Schouten, S. & Sinninghe Damsté, J. S. (2012b). Holocene subsurface temperature variability in the eastern Antarctic continental margin. *Geophysical Research Letters*, 39. doi 10.1029/2012GL051157.
- Kim J.-H., Schouten, S., Rodrigo-Gamiz, M., Rampen, S., Marino, G., Huguët, C., Helmke, P., Buscail, R., Hopmans, E. C., Pross, J., Sangiorgi, F., Middelburg, J. B. M., & Sinninghe Damsté J. S. (2015). Influence of deep-water derived isoprenoid tetraether lipids on the paleothermometer in the Mediterranean Sea. *Geochimica et Cosmochimica Acta*, 150, 125–141.
- Knappy, C. S., Chong, J. P., & Keely, B. J. (2009). Rapid discrimination of archaeal tetraether lipid cores by liquid chromatography-tandem mass spectrometry. *Journal of the American Society for Mass Spectrometry*, 20, 51–59.
- [Kumar, D. M., Woltering, M., Hopmans, E. C., Sinninghe Damsté, J. S., Schouten, S. & Werne, J. P. \(2019\). The vertical distribution of Thaumarchaeota in the water column of Lake Malawi inferred from core and intact polar tetraether lipids. *Organic Geochemistry* 132, 37–49.](#)
- Lawrence, K. T., Pearson, A., Castaneda, I. S., Ladlow, C., Peterson, L. C., Lawrence, G. E. (2020). Comparison of Late Neogene U^k₃₇ and TEX₈₆ Paleotemperature records from the eastern equatorial Pacific at orbital resolution. *Paleoceanography and Paleoclimatology*, 35, 1–16.
- Lengger, S.K., Hopmans, E.C., Reichart, G.-J., Nierop, K.G.J., Sinninghe Damsté, J.S., Schouten, S. (2012). Intact polar and core glycerol dibiphytanyl glycerol tetraether lipids in the Arabian Sea oxygen minimum zone. Part II: Selective preservation and degradation in sediments and consequences for the TEX₈₆. *Geochimica et Cosmochimica Acta* 98, 244–258.
- Lengger, S, K, Hopmans, E. C., Sinninghe Damsté, J. S., Schouten, S. (2014). Fossilization and degradation of archaeal intact polar tetraether lipids in deeply buried marine sediments (Peru Margin). *Geobiology*, 12(3), 212–220, <https://doi.org/10.1111/gbi.12081>.
- Lincoln, S. A., Wai, B., Eppley, J. M., Church, M. J., Summons, R. E., & DeLong, E. F. (2014). Planktonic euryarchaeota are a significant source of archaeal tetraether lipids in the ocean. *Proceedings of the National Academy of Sciences, U. S. A.* 111, 9858–9863. doi: 10.1073/pnas.1409439111.
- Lipp, J. S., & Hinrichs, K. U. (2009). Structural diversity and fate of intact polar lipids in marine sediments. *Geochimica et Cosmochimica Acta*, 73, 6816–6833.
- Lipp, J. S., Morono, Y., Inagaki, F., & Hinrichs, K. U. (2008). Significant contribution of Archaea to extant biomass in marine subsurface sediments. *Nature*, 454, 991–994.

- Liu, X. L., Leider, A., Gillespie, A., Gröger, J., Versteegh, G. J., & Hinrichs, K. U. (2010). Identification of polar lipid precursors of the ubiquitous branched GDGT orphan lipids in a peat bog in Northern Germany. *Organic Geochemistry*, 41, 653–660.
- Liu, X. -L., Lipp, J. S., Hinrichs, K. -U. (2011). Distribution of core and intact GDGTs in marine sediments. *Organic Geochemistry* 42, 368–375.
- Liu, X. L., Russell, D. A., Bonfio, C., Summons, R. E. (2018) Glycerol configurations of environmental GDGTs investigated using a selective sn2 ether cleavage protocol. *Organic Geochemistry*, 128, 57–62.
- Lopes dos Santos R. A., Prange M., Castaneda I. S., Schefuß E., Mulitza S., Schulz M., Niedermeyer E. M., Sinninghe Damsté J. S. and Schouten S. (2010). Glacial–interglacial variability in Atlantic meridional overturning circulation and thermocline adjustments in the tropical North Atlantic. *Earth and Planetary Science Letters*, 300, 407–414.
- Lunt, D. J., Haywood, A. M., Schmidt, G. A., Salzmann, U., Valdes, P. J., Dowsett, H. J., & Loptson, C.A. (2012). On the causes of mid-Pliocene warmth and polar amplification. *Earth and Planetary Science Letters*, 321–322, 128–138, doi:10.1016/j.epsl.2011.12.042.
- Ma, C., Coffinet, S., Lipp, J. S., Hinrichs, K. U., & Zhang, C. (2020). Marine Group II Euryarchaeota Contribute to the Archaeal Lipid Pool in Northwestern Pacific Ocean Surface Waters. *Frontiers in microbiology*, 11, 1034. <https://doi.org/10.3389/fmicb.2020.01034>.
- Macalady, J. L., Vestling, M. M., Baumler, D., Boekelheide, N., Kaspar, C. W., & Banfield, J. F. (2004). Tetraether-linked membrane monolayers in *Ferroplasma* spp: a key to survival in acid. *Extremophiles*, 8, 411–419.
- McClymont, E. L., Ganeshram, R. S., Pichevin, L. E., Talbot, H. M., van Dongen, B. E., Thunell, R. C., Haywood, A.M., Singarayer, J.S. & Valdes, P. J. (2012). Sea-surface temperature records of Termination 1 in the Gulf of California: Challenges for seasonal and interannual analogues of tropical Pacific climate change. *Paleoceanography*, 27, doi 10.1029/2011PA002226.
- McKay, L. J., MacGregor, B. J., Biddle, J. F., Albert, D. B., Mendlovitz, H. P., Hoer, D. R., Lipp, J.S., Lloyd, K.G & Teske, A. P. (2012). Spatial heterogeneity and underlying geochemistry of phylogenetically diverse orange and white Beggiatoa mats in Guaymas Basin hydrothermal sediments. *Deep Sea Research Part I: Oceanographic Research Papers*, 67, 21–31.
- Meyer, S., Wegener, G., Lloyd, K. G., Teske, A., Boetius, A., & Ramette, A. (2013). Microbial habitat connectivity across spatial scales and hydrothermal temperature gradients at Guaymas Basin. *Frontiers in Microbiology*, 4, 207.
- Morrissey, A., Scholz, C.A., & Russell, J.M. (2018). Late Quaternary TEX₈₆ paleotemperatures from the world's largest desert lake, Lake Turkana, Kenya. *Journal of Paleolimnology* 59, 103–117.
- Naafs, B. D. A., Rohrssen, M., Inglis, G. N., Lähteenoja, O., Feakins, S. J., Collinson, M. E., Kennedy, E.M., Singh, P.K., Singh, M.P., Lunt, D.J., & Pancost, R. D. (2018). High temperatures in the terrestrial mid-latitudes during the early Palaeogene. *Nature Geoscience*, 11, 766–771.
- O'Brien, C.L., Robinson, S.A. Pancost, R.D., Sinninghe Damste, J.S., Schouten, S., Lunt, D.J., Alsenz, H., Bomemann, A., Bottini, C., Brassell, S.C., Farnsworth, A., Forster, A., Huber, B.T., Inglis, G.N., Jenkyns, H.C., Linnert, C., Littler, K., Markwick, P., McAnena, A., Mutterlose, J., Naafs, B.D.A., Puttmann, W., Sluijs, A., van Helmond, N.A.G.M., Vellekoop, J., Wagner, T., & Wrobel, N.E. (2017). Cretaceous sea-surface temperature evolution: Constraints from TEX₈₆ and planktonic foraminiferal oxygen isotopes. *Earth-Science Reviews*. 172, 224–247.

- Pearson, A. & Ingalls, A. E. (2013) Assessing the use of archaeal lipids as marine environmental proxies. *Annual Review Earth Planetary Science*. 41, 15.1–15.26.
- Pearson, A., Huang, Z., Ingalls, A. E., Romanek, C. S., Wiegel, J., Freeman, K. H., Smittenberg, R. H. & Zhang, C. L. (2004). Nonmarine crenarchaeol in Nevada hot springs. *Applied and Environmental Microbiology*, 70, 5229–5237.
- Petrack, B., Reuning, L., & Martinez-Garcia (2019) Distribution of Glycerol Dialkyl Glycerol Tetraethers (GDGTs) in Microbial Mats From Holocene and Miocene Sabkha Sediments. *Frontiers in Earth Science*. 04. doi.org/10.3389/feart.2019.00310.
- Powers, L., Werne, J. P., Vanderwoude, A. J., Sinninghe Damsté, J. S., Hopmans, E. C., & Schouten, S. (2010). Applicability and calibration of the TEX₈₆ paleothermometer in lakes. *Organic Geochemistry*, 41, 404–413.
- Qin, W., Carlson, L. T., Armbrust, E. V., Devol, A. H., Moffett, J. W., Stahl, D. A., & Ingalls, A. E. (2015). Confounding effects of oxygen and temperature on the TEX₈₆ signature of marine Thaumarchaeota. *Proceedings of the National Academy of Sciences, U. S. A.* 112(35), 10,979–10,984. doi.org/10.1073/pnas.1501568112.
- Robinson, S. A., Ruhl, M., Astley, D. L., Naafs, B. D. A., Farnsworth, A. J., Bown, P. R., Jenkyns, H. C., Lunt, D. J., O'Brien, C., Pancost, R. D., & Markwick, P. J. (2017). Early Jurassic North Atlantic sea-surface temperatures from TEX₈₆. *Palaeothermometry. Sedimentology*. 64, 215–230.
- Rommerskirchen, F., Condon, T., Mollenhauer, G., Dupont, L. M., & Schefuß, E. (2011). Miocene to Pliocene development of surface and subsurface temperatures in the Benguela Current system. *Paleoceanography*, 26, PA3216, 1–15. doi.org/10.1029/2010PA002074.
- Schouten, S., Hopmans, E. C., & Sinninghe Damsté, J. S. (2013). The organic geochemistry of glycerol dialkyl glycerol tetraether lipids: A review. *Organic Geochemistry*, 54, 19–61.
- Schouten, S., Hopmans, E. C., & Sinninghe Damsté, J. S. (2004). The effect of maturity and depositional redox conditions on archaeal tetraether lipid palaeothermometry. *Organic Geochemistry*, 35, 567–571.
- Schouten, S., Hopmans, E. C., Schefuß, E., & Sinninghe Damsté, J. S. (2002). Distributional variations in marine crenarchaeotal membrane lipids: a new tool for reconstructing ancient sea water temperatures? *Earth and Planetary Science Letters*, 204, 265–274.
- Schouten S., Wakeham S. G., Hopmans E. C. and Sinninghe Damsté J. S. (2003) Biogeochemical Evidence that Thermophilic Archaea Mediate the Anaerobic Oxidation of Methane. *Appl. Environ. Microbiol.* 69, 1680–1686.
- Seki, O., Bendle, J. A., Haranda, N., Kobayashi, M., Sawada, K., Moossen, H., Inglis, G. N., Nagao, S., & Sakamoto, T. (2014). Assessment and calibration of TEX₈₆ paleothermometry in the Sea of Okhotsk and sub-polar North Pacific region: Implications for paleoceanography. *Progress in Oceanography*. 126, 254–266.
- Sinninghe Damsté, J. S., Ossebaard, J., Abbas, B., Schouten, S., & Verschuren, D. (2009). Fluxes and distribution of tetraether lipids in an equatorial African lake: constraints on the application of the TEX₈₆ palaeothermometer and BIT index in lacustrine settings. *Geochimica et Cosmochimica Acta*, 73, 4232–4249.
- Sinninghe Damsté J. S., Rijpstra W. I. C., Hopmans E. C., den Uijl M. J., Weijers J. W. H. and Schouten S. (2018) The enigmatic structure of the crenarchaeol isomer. *Organic Geochemistry* 124, 22–28.

Formatted: Indent: Left: 0 cm, First line: 0 cm

- Stadnitskaia, A., Nadezhkin, D., Abbas, B., Blinova, V., Ivanov, M. K., & Sinninghe Damsté, J. S. (2008). Carbonate formation by anaerobic oxidation of methane: evidence from lipid biomarker and fossil 16S rDNA. *Geochimica et Cosmochimica Acta*, 72(7), 1824–1836.
- Sturt, H. F., Summons, R. E., Smith, K., Elvert, M., & Hinrichs, K. U. (2004). Intact polar membrane lipids in prokaryotes and sediments deciphered by high-performance liquid chromatography/electrospray ionization multistage mass spectrometry—new biomarkers for biogeochemistry and microbial ecology. *Rapid communications in mass spectrometry*, 18, 617–628.
- Teske, A., Callaghan, A. V., & LaRowe, D. E. (2014). Biosphere frontiers of subsurface life in the sedimented hydrothermal system of Guaymas Basin. *Frontiers in Microbiology*, 5, 362.
- Teske, A., De Beer, D., McKay, L. J., Tivey, M. K., Biddle, J. F., Hoer, D., Lloyd, K.G., Lever, M.A., Røy, H., Albert, D.B & MacGregor, B. J. (2016). The Guaymas Basin hiking guide to hydrothermal mounds, chimneys, and microbial mats: Complex seafloor expressions of subsurface hydrothermal circulation. *Frontiers in Microbiology*, 7, 75.
- Tierney, J. E. (2014). Biomarker-based inferences of past climate: the TEX₈₆ paleotemperature proxy. In H.D. Holland & K.K. Turekian (Eds.) *Treatise on Geochemistry* (2nd Ed.) 12, 379–939.
- Uda, I., Sugai, A., Itoh, Y. H., & Itoh, T. (2001). Variation in molecular species of polar lipids from *Thermoplasma acidophilum* depends on growth temperature. *Lipids*, 36, 103–105.
- Umoh, U., Li L., Luckge, A., Schwartz-Schampera, U., & Naafs, D. (2020). Influence of hydrothermal vent activity on GDGT pool in marine sediments might be less than previously thought. *Organic Geochemistry*. 104102. doi.org/10.1016/j.orggeochem.2020.104102.
- Wakeham, S. G., Lewis, C. M., Hopmans, E. C., Schouten, S., & Sinninghe Damsté, J. S. (2003). Archaeal mediate anaerobic oxidation of methane in deep euxinic waters of the Black Sea. *Geochimica et Cosmochimica Acta*, 67, 1359–1374.
- Wang, J. X., Wei, Y., Wang, P., Hong, Y., & Zhang, C. L. (2015). Unusually low TEX₈₆ values in the transitional zone between Pearl River estuary and coastal South China Sea: impact of changing archaeal community composition. *Chemical Geology*, 402, 18–29. doi: 10.1016/j.chemgeo.2015.03.002.
- Weijers, J. W., Schefuß, E., Kim, J. H., Sinninghe Damsté, J. S., & Schouten, S. (2014). Constraints on the sources of branched tetraether membrane lipids in distal marine sediments. *Organic Geochemistry*, 72, 14–22.
- Weijers, J. W., Schouten, S., van den Donker, J. C., Hopmans, E. C., & Sinninghe Damsté, J. S. (2007). Environmental controls on bacterial tetraether membrane lipid distribution in soils. *Geochimica et Cosmochimica Acta*, 71, 703–713.
- Wuchter, C., Schouten, S., Wakeham, S. G., & Sinninghe Damsté, J. S. (2005). Temporal and spatial variation in tetraether membrane lipids of marine Crenarchaeota in particulate organic matter: Implications for TEX₈₆ paleothermometry. *Paleoceanography*, 20, doi 10.1029/2004PA001110.
- Wuchter, C., Schouten, S., Wakeham, S. G. & Sinninghe Damsté, J. S. (2006). Archaeal tetraether membrane lipid fluxes in the northeastern Pacific and the Arabian Sea: implications for TEX₈₆ paleothermometry. *Paleoceanography* 21.
- Yao, Y., Zhao, J., Bauersachs, T., & Huang, Y. (2019). Effect of water depth on the TEX₈₆ proxy in volcanic lakes of northeastern China. *Organic Geochemistry* 129, 88–89.

1083 Yoshinaga, M. Y., Kellermann, M. Y., Rossel, P. E., Schubotz, F., Lipp, J. S., & Hinrichs, K. U. (2011).
 1084 Systematic fragmentation patterns of archaeal intact polar lipids by high-performance liquid
 1085 chromatography/electrospray ionization ion-trap mass spectrometry. *Rapid Communications in Mass*
 1086 *Spectrometry*, 25, 3563–3574.
 1087
 1088 Zeng, Z., Liu, X. L., Farley, K. R., Wei, J. H., Metcalf, W. W., Summons, R. E., & Zhang, Y. G., Pagani,
 1089 M., & Wang, Z. (2016). Ring Index: A new strategy to evaluate the integrity of TEX₈₆
 1090 paleothermometry. *Paleoceanography*, 31, 220–232.
 1091
 1092 Zhang, Y. G., Zhang, C. L., Liu, X. L., Li, L., Hinrichs, K. U., & Noakes, J. E. (2011). Methane Index: A
 1093 tetraether archaeal lipid biomarker indicator for detecting the instability of marine gas hydrates. *Earth*
 1094 *and Planetary Science Letters*, 307, 525–534.
 1095
 1096 Zhang, Y. G., Pagani, M. & Wang, Z. (2016). Ring Index: A new strategy to evaluate the integrity of
 1097 TEX₈₆ paleothermometry. *Paleoceanography and Paleoclimatology* 31:220–232, doi.org/
 1098 10.1002/2015PA002848.
 1099
 1100 Zhu, C., Lipp, J. S., Wörmer, L., Becker, K. W., Schröder, J., & Hinrichs, K. U. (2013). Comprehensive
 1101 glycerol ether lipid fingerprints through a novel reversed phase liquid ~~chromatography–~~
 1102 ~~mass~~chromatography-mass spectrometry protocol. *Organic Geochemistry*, 65, 53–62.